Composites Science and Technology 250 (2024) 110514

Contents lists available at ScienceDirect

Composites Science and Technology

journal homepage: www.elsevier.com/locate/compscitech

Mechanical characterization of polymer-grafted graphene PEG nanocomposites using molecular dynamics

Cátia Guarda [a], Bruno Faria [b], José N. Canongia Lopes [a], Nuno Silvestre [c,*]

[a] CQE – Centro de Química Estrutural, Institute of Molecular Sciences, Instituto Superior Técnico, Universidade de Lisboa, Portugal
[b] IPC – Institute for Polymers and Composites, Polymer Engineering Department, University of Minho, Portugal
[c] IDMEC – Institute of Mechanical Engineering, Department of Mechanical Engineering, Instituto Superior Técnico, Universidade de Lisboa, Portugal

ARTICLE INFO

Keywords:
Functionalized graphene
Polyethylene glycol (PEG) nanocomposites
Compression
Tension
Mechanical properties

ABSTRACT

It is known that most polymers exhibit poor interfacial compatibility with graphene sheets. Modification of graphene's surface by functionalization with small polymer chains from the same building blocks as the matrix polymer improves the compatibility of graphene in polymeric materials. In this paper, the mechanical behaviour of polyethylene glycol (PEG) nanocomposites with graphene grafted with polymeric chains under tensile and compression is investigated using molecular dynamics. The influence of the functional groups (-NH_2 and –OH) that bond the polymer chain to graphene is analysed. It is found that the system containing the –NH_2 functional group showed lower mechanical properties than the system containing the –OH functional group. The mechanical properties of five PEG-nanocomposites are investigated: PEG/G, PEG/GNH-1PEG-S, PEG/GNH-2PEG-L, PEG/GNH-1PEG-S-NH_2, PEG/GO-1PEG-S. The radius distribution function values and the variation of interfacial interaction energy are also examined. It is shown that functionalization of the graphene sheet increases the magnitude of the interaction energy, and it also reveals higher adhesion between graphene surface and PEG matrix. It is found that the mechanical properties of PEG are mostly improved in the longitudinal direction (reinforcement up to 43 %). Despite the high interaction between the nanofiller and PEG matrix, the low intrinsic properties of the nanofiller, namely Young's modulus, as well as the rupture of the graphene sheet during the deformation process deteriorated the mechanical properties of the nanocomposite. The presence of polymeric chains grafted to graphene improves the adhesion between the graphene surface and the polymeric matrix but decreases its mechanical properties.

1. Introduction

The combination of graphene-based nanomaterials and polymers resulted in a new class of materials called polymeric nanocomposites [1–4]. A major reason for using graphene as nanofiller is its large surface-to-volume ratio, which increases the intrinsic properties of polymeric materials. The large interfacial area between graphene nano-sized heterogeneities and the polymer matrix can lead to improved mechanical properties. To achieve the maximum increase of nanocomposite properties, graphene flakes should be homogeneously dispersed into the polymer matrix and the external load efficiently transferred through strong nanofiller/polymer interfacial interactions. However, it is known that strong van der Waals (vdW) forces between graphene layers results in poor compatibility with most polymers. Furthermore, carbon atoms of graphene are chemically stable due to the aromatic nature of C–C bonds. As a result, reinforcing phases of graphene are usually inert and interact with the surrounding matrix mainly through vdW interactions. These weak interactions are unable to provide efficient load transfer across graphene/polymer interfaces [5]. To achieve a good mechanical performance of polymer nanocomposites, it is deemed necessary to chemically modify the graphene surface so it can disperse homogeneously into the matrix and improve its compatibility with polymers [6–8].

Up to now, most of the available studies have focused on the modification of graphene via functionalization. Functionalized graphene offers many advantages as nanofiller for polymer nanocomposites because (i) it holds most of the physical properties of graphene, and (ii) the functionalities on graphene's surface increase its dispersion in polymeric matrices and enhance the interfacial interaction between graphene and polymers [9–12].

* Corresponding author.
E-mail address: nsilvestre@tecnico.ulisboa.pt (N. Silvestre).

https://doi.org/10.1016/j.compscitech.2024.110514
Received 6 July 2023; Received in revised form 12 February 2024; Accepted 23 February 2024
Available online 28 February 2024

Another effective, but less explored approach, to improve the dispersion and compatibility of graphene in polymers is to directly functionalize graphene with polymer chains identical (or structurally similar) to the matrix polymers [6,13–16]. The introduction of well-defined polymer chains on the surface of graphene sheets allows the preparation of composites that merge the properties of the polymer with the conductivity and strength of graphene. Recently, Vallés et al. [17] investigated the mechanical and thermal properties of poly(methyl methacrylate) (PMMA) composites with PMMA-grafted graphene nanoplatelets. These authors demonstrated that 2 wt% of nanofiller in PMMA was found to increase the elastic modulus, strength, and failure strain of PMMA, whereas the incorporation of unmodified graphene nanoplatelets showed poor levels of reinforcement. Wang et al. [18] also reported that poly(l-lactic acid)-grafted graphene oxide (GO-g-PLA) can disperse homogeneously in the PLA matrix, and showed that the mechanical properties of GO-g-PLA/PLA were superior to that of GO/PLA. In particular, 3 % GO-g-PLA content yielded a 37.8 % increase in the tensile strength of PLA composites. Yang and Zhen [19] also incorporated graphene oxide grafted with polystyrene (SGO-PS) in a PLA matrix and studied the properties of the resulting nanocomposite (PLA/S-GO-PS). The mechanical properties of the PLA/SGO-PS (0.3 wt%) nanocomposites reached a tensile strength of 82.56 MPa (8 % higher than pure PLA). However, with further increase of SGO-PS content, the mechanical properties of PLA nanocomposites gradually decreased. According to the authors, a small amount of SGO-PS can be evenly dispersed in the PLA matrix allowing a strong interaction with the PLA matrix. However, when the content of SGO-PS is higher than 0.3 wt%, the mechanical properties of PLA/SGO-PS nanocomposites decreased rapidly, most likely due to decreased dispersion, heterogeneity, and anisotropy of SGO-PS in the matrix. Chen et al. [20] investigated the mechanical properties of PLA nanocomposites incorporating thermally reduced graphene oxide (TRG), TRG-g-PMMA, and TRG-g-polyvinyl acetate (PVAc). Their findings demonstrated that PLLA nanocomposites with TRG-g-PMMA and TRG-g-PVAc exhibited improved elongation at the breaking point while maintaining tensile strength and modulus. This enhanced toughness was attributed to PMMA and PVAc chain grafting on TRG, enabling better dispersion in the PLLA matrix and restricting TRG's nucleation properties. Pour and Ghaemy [21] examined composites of epoxy resin with pristine graphene oxide (GO), silane-functionalized GO (I-GO), and PVI-grafted GO (PVI-g-GO) nanosheets. Their study revealed substantial enhancements in both tensile strength (59.6% increase) and modulus (45.5% increase) compared to neat epoxy (EP). Furthermore, the nanocomposites exhibited improved thermal stability. In a similar study, but using rolled graphene sheets, *i.e.*, carbon nanotubes (CNT), Wang et al. [22] employed a covalent functionalization method to graft hyperbranched poly (trimellitic anhydride-diethylene glycol) ester epoxy resin (HTDE) onto multiwalled carbon nanotubes (MWCNTs). These HTDE-grafted MWCNTs (HTDE-g-MWCNTs) were then used to enhance epoxy composites (HTDE-g-MWCNT/EP). The results demonstrated that the HTDE-g-MWCNTs were uniformly dispersed within the epoxy matrix, resulting in improved tensile strength and fracture toughness in the HTDE-g-MWCNT/EP composites.

To shed light on the experimental findings of polymer nanocomposites reinforced with polymer grafted graphene, a molecular-level understanding of the behaviour of these systems using computational models has been increasingly required. Liu et al. [23] studied the interfacial mechanical properties between graphene functionalized with polymer chains and a polyethylene (PE) matrix. The results indicated that grafting short PE molecular chains onto graphene significantly enhances interfacial shear strength and interfacial fracture toughness in functionalized graphene/PE nanocomposites. Grafting density and chain length have notable impacts on interfacial mechanical properties. The study also revealed that the interfacial cohesive strength decreases with increasing grafting density and chain length, while interfacial shear strength increases with grafting density for short grafting chains but decreases with longer chains. The interfacial fracture toughness is significantly enhanced for long grafting PE chains, making graphene functionalized with PE chains, especially short ones, exhibit higher interfacial fracture toughness. Gotebiowski et al. [24] investigated the pullout of CNT from a crosslinked PE matrix. They explored various functional groups that bind the polymer to the CNT, including amine, carbene, carboxyl and a [2 + 1] cycloaddition. The choice of functional group significantly influenced the strength of the interface, with the [2 + 1] cycloaddition leading to the strongest interface, which was 50 % stronger and 70 % stronger than other cases. In this work, molecular dynamics (MD) simulations are used to provide (i) a comprehensive characterization of the mechanical properties of four graphene sheets grafted with polyethylene glycol (PEG) chains of various lengths; and (ii) a study on the mechanical behaviour of PEG nanocomposites containing the previously studied PEG-grafted graphene sheets.

2. Computational approach

2.1. Polymer-grafted graphenes

2.1.1. Structure and configurations

MD simulations were performed to evaluate the mechanical properties of four PEG polymer-grafted graphene under tensile and compressive loading. Pristine graphene was also modelled for comparative purposes. Pristine graphene sheets consisting of 396 atoms were modelled, with length, L = 37.5 Å, and width, W = 26.2 Å. The thickness of the sheets is the accepted vdW distance for graphene interplanar spacing (3.4 Å) [25,26]. PEG polymer chains with two different lengths were grafted onto graphene: (i) PEG chain with a length of 17 Å, consisting of 5 monomers (C_2H_4O) and (ii) PEG chain with a length of 29 Å, composed of 9 monomers (C_2H_4O). The PEG chain with 17 Å is referred here as "short chain" and the PEG chain with 29 Å as "long chain". Both the short PEG chain and the long PEG chain were then grafted to the graphene sheet in various configurations, described below. In addition to pristine graphene sheets grafted with PEG chains (Fig. 1a),), this work also considers the effect of grafting on functionalized graphene sheets. Thus, PEG chains were grafted in graphene sheets functionalized with $–NH_2$ (Fig. 1b)) and –OH groups (degree of functionalization of 10 %). Finally, the grafting mechanism was also studied by replacing the terminal "group" connecting the PEG chain to graphene by –NH (Fig. 1 c) and d)). Overall, factors such as chain size, number of grafted chains, type of functionalization of graphene sheets and the polymer-graphene bonding were investigated in detail. To avoid lengthy descriptions of the type of system studied, the following abbreviations (labels) were adopted.

- Type of bonding between PEG and graphene: GO (default oxygen bonding) or GNH (nitrogen bonding);
- Number and type of grafted polymer chains: 1PEG (one chain of PEG) or 2PEG (two chains of PEG, one per side of graphene sheet);
- Length of polymer chain: S (short) or L (Long);
- Type of graphene functionalization OH or NH_2.

For illustration purpose, GNH-1PEG-S-NH_2 stands for one PEG short chain grafted by NH bonding to a NH_2 functionalized graphene sheet.

Fig. 1 shows the four types of systems: (a) graphene grafted with one short PEG chain (GO-1PEG-S); (b) graphene functionalized with $–NH_2$ and grafted with one short PEG chain bonded by –NH to graphene (GNH-1PEG-S-NH_2); (c) graphene grafted with one short PEG which is bonded by –NH to graphene (GNH-1PEG-S) and (d) graphene grafted with two long PEG chains bonded by –NH on opposite sides of the sheet (GNH-2PEG-L). To avoid the unsaturated boundary effect, hydrogen atoms were added at the edges of the polymer grafted-graphene sheets, however they were neither counted nor represented in Fig. 1 for simplification purposes. The systems data, concerning the number of polymer chains (N) and size of polymer chain (L_p) are presented in Table 1.

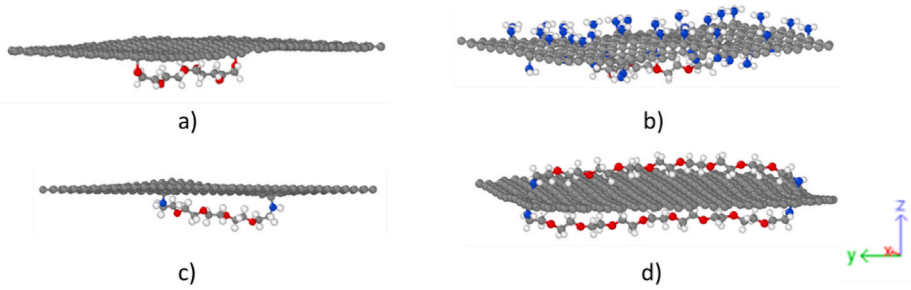

Fig. 1. Representative simulation models of PEG-grafted graphene: (a) GO-1PEG-S; (b) GNH-1PEG-S-NH_2, (c) GNH-1PEG-S, (d) GNH-2PEG-L.

Table 1
Systems data, where N is the number of polymer chains and L_p is the size of polymeric chain.

Systems	N	L_p (Å)
PEG/GNH-1PEG-S	1	17
PEG/GNH-2PEG-L	2	29
PEG/GNH-1PEG-S-NH_2[a]	1	17
PEG/GO-1PEG-S	1	17

[a] Graphene sheet functionalized with 10 % –NH_2.

2.1.2. Forcefields and MD methodology

The polymer-grafted graphene sheets were mechanically tested using the ReaxFF potential, with parameterization proposed by Vashisth et al. [27]. For all simulations, a timestep of 0.1 fs and non-periodic boundary conditions were applied. This value for the timestep is within the range suggested by Jensen et al. [28] for this potential to provide consistent results in simulations of graphenic structures under mechanical loading. The Nosé-Hoover thermostat with a damping parameter of 100 fs was employed. All simulations were performed with LAMMPS (Large Scale Massive Atomic/Molecular Simulator) [29] in the context of the canonical ensemble for NVT. The temperature was kept constant at 100 K.

2.1.3. Mechanical loadings tests

The initial configurations of polymer-grafted graphene sheets were optimized using the conjugate gradient algorithm with energy and force tolerances of 10^{-12} and subsequently equilibrated for 10 ps at 100 K. Both tensile and compressive loadings were applied to "fixed" (non-thermostated) atoms on the top and bottom ends of the sheets (represented in green in Fig. 2). Their motion was confined to the y-axis with a prescribed velocity. Tensile and compressive loads were simulated by assigning inward opposite velocities to these fixed atoms at both edges. This loading method was first used to mechanically test pristine graphene and obtain validation of the method by comparison with published results.

For tensile loading, a displacement velocity of 1 Å/ps was imposed to the fixed atoms at both edges but with outward opposite directions along the y-axis (length direction). Both edges were simultaneously pulled apart at a strain rate of 2.7×10^{10} s^{-1}. Globally, the sheets were stretched by 20 Å, eventually leading to rupture before reaching the final length.

For compressive loading, a displacement velocity also of 1 Å/ps was imposed to the fixed atoms at both edges but in inward opposite directions. Both edges were simultaneously pushed towards the middle of the sheet at a strain rate of 2.7×10^{10} s^{-1}. Here, sheets were compressed by 20 Å and deformed. The strain rate used here was selected by comparing the results obtained from slower and faster strain rates for GO-1PEG-S (see Appendix A). It was concluded that 2.7×10^{10} s^{-1} is the fastest strain rate within the range of strain rates that would produce reasonable results. The virial stress method was used to calculate the total stress using: $\sigma_{ab} = S_{ab}\Omega^{-1}$, where Ω is the representative volume and S_{ab} is the stress tensor. Different approaches have been developed to calculate stress in atomistic simulations [30–32]In LAMMPS, the virial stress approach (based on the generalized virial theorem of Clausius [33]) is adopted. Although some controversy exists whether to include the kinetic contribution to the virial stress or to consider only the potential contribution [34–36], it is generally accepted that the virial stress is equivalent to the continuum Cauchy stress, provided that sufficient spatial and temporal averaging is employed [35]. AMMPS calculates atomic stress in the form of a symmetric 6 component stress tensor that, for atom i, is given by the following virial stress expression:

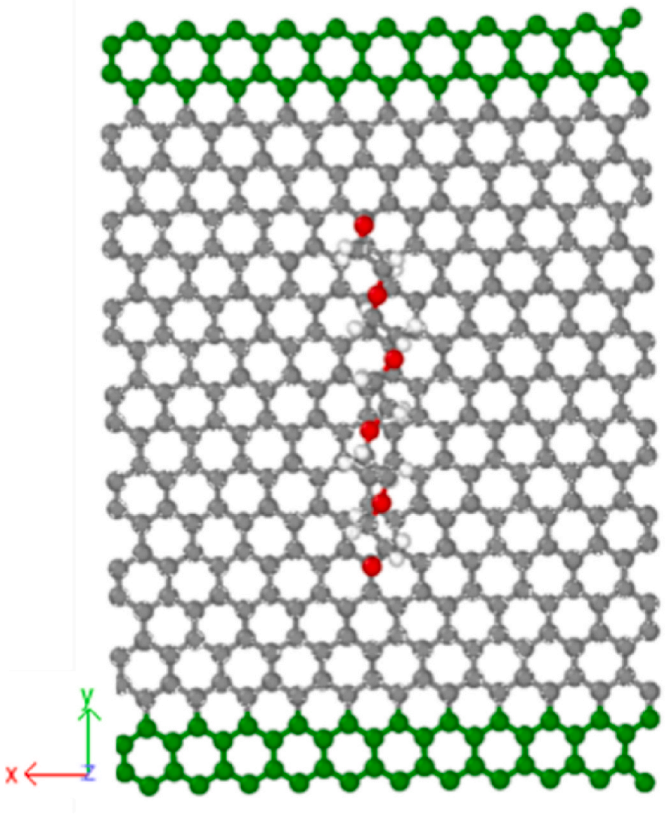

Fig. 2. Representation of the boundary conditions (green atoms) applied to polymer-grafted graphene GO-1PEG-S.

$$S_{ab} = -\left[mv_a v_b + \frac{1}{2}\sum_{n=1}^{Npair}(r_{1a}F_{1b} + r_{2a}F_{2b}) + \frac{1}{2}\sum_{n=1}^{Nbonds}(r_{1a}F_{1b} + r_{2a}F_{2b}) + \frac{1}{3}\sum_{n=1}^{Nangles}(r_{1a}F_{1b} + r_{2a}F_{2b} + r_{3a}F_{3b}) \right] \quad (1)$$

where a and b assume the corresponding x,y and z values. The first term, where m is the mass for atom i and v is the velocity component of the Cartesian coordinate, represents the kinetic energy contribution for

atom i. The second term represents the energy contribution from pairwise interactions between the Npair neighbours of atom i, and where r1 and F1, and r2 and F2 represent the positions and forces acting on the two atoms resulting from the pairwise interaction. Since stress had to be calculated for nanostructures modelled by manybody potentials (such as AIREBO, ReaxFF) but also for conventional potentials such as OPLS, where bonds and angles were specified, the virial stress expression includes two additional terms. Hence, the third term is the bond energy contribution (defined similarly to the pairwise energy contribution) for the Nbonds in which atom i participates and the fourth term refers to the angle contribution, also similarly defined, for the Nangles that atom i is part of. Note that atomic stress, as defined in eq. (1), is given in stress. volume units. In the simulations presented in this work, only tensile and compressive deformations were implemented, thus atomic stress can be reasonably approximated by calculating Syy (y is the loading direction). The total stress can then be obtained by the sum of atomic stresses Syy for all N atoms in consideration. Once total stress is obtained for each timestep, effective stress can be calculated from time averaging over a prescribed number of simulation steps, collected at a selected frequency, during the simulation. However, given that effective stress has a stress. volume formulation, it has to be divided by the total volume of the nanostructure in consideration. The volume was obtained by summing the volume of the sheet with a thickness of 3.4 Å [25,26] with the volume of the polymer. The latter was calculated by approximation to the volume of a cylinder, where the radius corresponds to the length of the C–H bond. Appendix C (Fig. C1 and Table C4) includes a comparison between two different methods for obtaining volume required for stress calculation. Graphene volume can be obtained by the usual method described here or by a different method where volume is calculated using the Voronoi tessellation method. The two methods not equivalent because the Voronoi method can give a more accurate polymer chain volume, but differences are small. On the other hand stress-strain curves become much "noisier", and the mechanical properties are more difficult to obtain. In view of this, here the usual method is applied. The Young's modulus (Y) and ultimate stress (σ_{ult}) were obtained from the stress-strain curves. The Young's modulus was calculated as the initial slope of the stress-strain curve, in the range $0 < \varepsilon_y < 0.05$. The ultimate stress was achieved at the peak stress-strain curve [37].

2.2. Polymer nanocomposites

2.2.1. Structure and configurations

Four PEG nanocomposites were constructed: PEG/GNH-1PEG-S, PEG/GNH-2PEG-L, PEG/GNH-1PEG-S-NH_2, PEG/GO-1PEG-S. The PEG/pristine graphene (PEG/G) nanocomposite was also modelled for comparative purposes. All the five systems were constructed using similar protocols. The initial configuration of the PEG-nanocomposites (Fig. 3)was constructed by randomly placing 130 PEG molecular chains (60 PEG chains with 10 monomers, 40 PEG chains with 20 monomers, 20 PEG chains with 40 monomers, and 10 PEG chains with 60 monomers) into a cubic simulation box with dimensions of 20 × 20× 20 nm^3. The nanofillers were embedded at the center of this box. The final target density of the nanocomposites was set at 1.17 g cm^{-3} [38,39]. Thus, after the initial preparation of the nanocomposites, the system was equilibrated for 50 ps in the NVT ensemble at a temperature of 300 K. Subsequently, an NPT simulation was performed for 100 ps at a temperature and pressure of 300 K and 50.7 KPa, respectively.

Finally, successive deformations in the simulation box were performed, for 100 ps using the NVT ensemble at 300 K. The deformations allowed to change the dimensions of the simulation box at constant engineering strain rate to achieve the final target density. Between each deformation, the systems were equilibrated for 50 ps on the NVT ensemble to achieve a thermodynamically balanced structure. Consequently, the target density increased until the final target density was

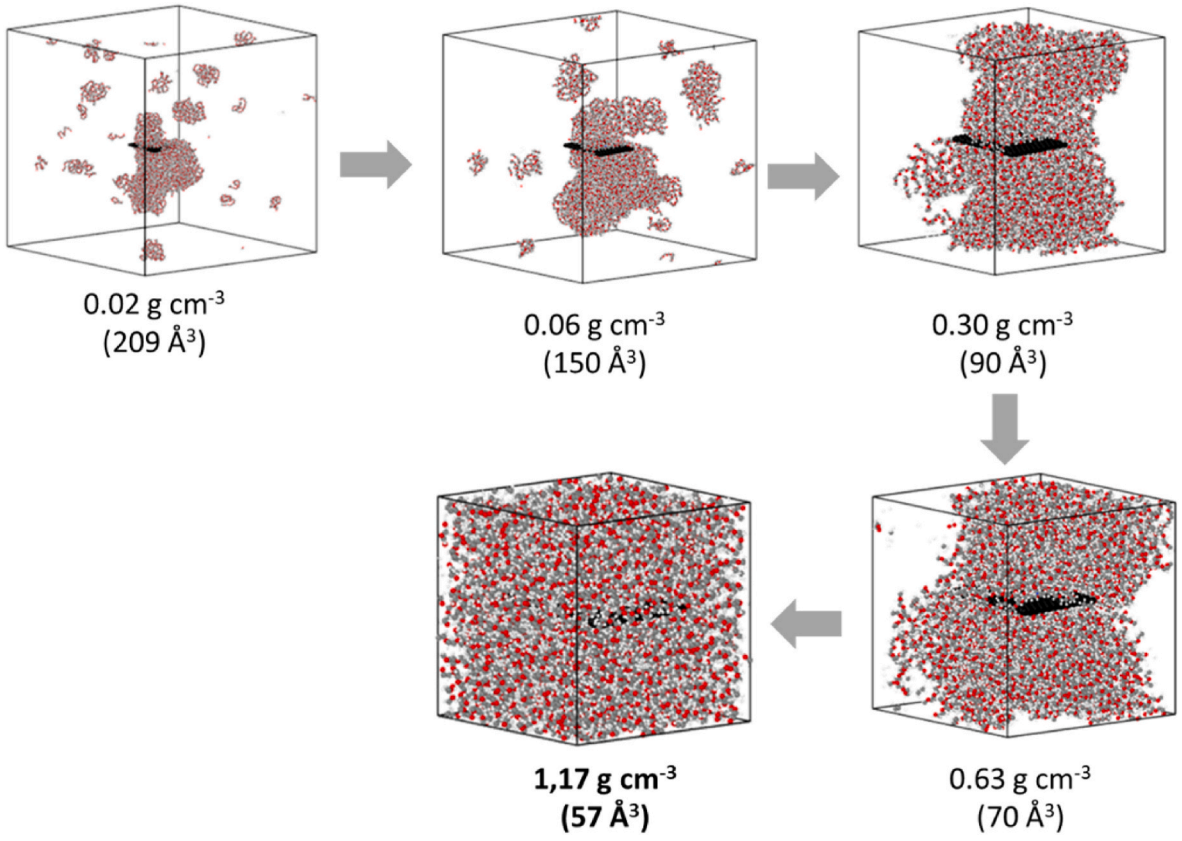

Fig. 3. Representative scheme of the stages for obtaining the final target density of the PEG/GNH-1PEG-S nanocomposite. Grey, red, white, blue and dark grey colours denote C, O, H atoms of PEG and N and C of nanofiller, respectively.

reached. Periodic boundary conditions were applied in all simulations. Information on the nanocomposites is listed in Table 2. LAMMPS software [29] was also used to conduct the MD simulations. The presented method for obtaining the final target density was first used to the pristine PEG, which allowed the method to be validated by comparing the density obtained with the published values [39,40].

2.2.2. Forcefields and MD methodology

The AIREBO potential [41] was applied here to describe the C–C bond interactions within graphene. Since O and N interactions cannot by modelled by AIREBO, the OPLS-AA (all-atom optimized potential for liquid simulations) force field [42] was chosen to describe C–O–H interactions, in accordance with Hughes et al. [43] and C–N–H interactions as suggested by Dasetty et al. [44], thus apart from C–C interactions from graphene, all bonded interactions were modelled by OPLS-AA. The Lennard-Jones (LJ) 12–6 interaction potential was applied to calculate the non-bonded interactions. The LJ parameters for the interactions between PEG atoms (C, O and H), functional groups (N, H, C, O) and C atoms of graphene are calculated by the Lorentz-Bertholet mixing rule [45]:

$$\varepsilon_{a-b} = \sqrt{\varepsilon_{a-a}\,\varepsilon_{b-b}} \tag{1}$$

$$\sigma_{a-b} = \frac{1}{2}(\sigma_{a-a} + \sigma_{b-b}) \tag{2}$$

where ε and σ are the coefficient of well-depth energy and the equilibrium distance of null potential, respectively. The value of ε_{a-b} was obtained from Eq. (1) using ε_{a-a} (C, graphene) and ε_{b-b} (C, O and H, PEG). The value of σ_{a-b} was obtained from Eq. (2) using σ_{a-a} (C, graphene) and σ_{b-b} (C, O and H, PEG). Table 3 summarizes the LJ well-depth (ε) and interatomic distance (σ) parameter values for C–C (graphene) taken from Ref. [46] and the parameters for C–C (PEG), N–N, O–O and H–H non-bonded interactions included in LAMMPS package [45] for OPLS-AA potential. A cutoff distance of 12.0 Å was chosen for the LJ interfacial interactions.

2.2.3. Mechanical loadings tests

In a previous study, Hossain et al. [47] investigated the deformation mechanisms during uniaxial tensile deformation of an amorphous polyethylene polymer. Before deforming the amorphous polymer, they performed an equilibration sequence, which involved relaxation and cooling steps. After equilibration, they applied a constant strain rate with a zero-pressure condition to the two lateral simulation cell faces. In addition to investigating the effects of varying chain length and number, the authors also analysed the strain rate and temperature dependence of the stress-strain behaviour. Since the glass transition temperature, T_g, is an important characteristic of polymeric material, they chose three different temperatures: 100 K (low temperature), 250 K (temperature just below the T_g) and 400 K (temperature above the T_g) for the simulations. The MD results of this study showed that the most favourable conditions to obtain accurate mechanical properties of this type of polymers are a temperature around 100 K and a maximum strain rate of 10^9 s^{-1}. Here, a deformation approach similar to that of Hossain et al. [47] was applied. After obtaining the final target density and prior to deforming the PEG-nanocomposites, an equilibration sequence was performed to relax abnormal high energy configurations that are artificially created when obtaining the final polymer structure. The relaxation involved three different steps. Initially, the simulation ran for 50 ps using a NVT ensemble at 300 K. Then, the system's temperature was decreased from 300 K to 100 K at a cooling rate of 0.8 K/ps for 250 ps, using a NPT ensemble. The cooling rate used was the same as adopted by Hossain et al. [47]. Finally, the systems were relaxed for 25 ps at a temperature of 100 K.

Table 3
LJ parameters for C–C (graphene) [46], C–C (PEG), N–N, O–O and H–H [45].

Non-bonded interaction	ε (eV)	σ (Å)
C–C (graphene)	0.00296	3.407
C–C (PEG)	0.00512	3.905
N–N	0.00737	3.300
O–O	0.00737	3.007
H–H	0.00130	2.500
H–H[a]	0.00000	0.000
C–C[b]	0.00915	4.289

[a] H of the terminal –OH group of PEG.
[b] C bonded to N.

Next, the systems were deformed under uniaxial tension applied at a constant strain rate of 1.0×10^{10} s^{-1} (displacement velocity of 0.59 Å/ps) with zero-pressure condition for the two lateral simulation cell faces. This deformation condition was implemented in LAMMPS by decoupling the boundary in the loading direction from the NPT equations of motion [47,48]. Similarly to the case of choosing an appropriate strain rate for polymer grafted graphenes, also here the strain rate used was selected by comparing the results obtained from slower and faster strain rates for PEG-graphene nanocomposite (see Appendix A). It was concluded that $1{,}0 \times 10^{10}$ s^{-1} is the fastest strain rate within the range of strain rates that would produce reasonable results. In this context, reasonable results refer to results that exhibit little variation across the range of strain rates considered here and typically studied in polymeric nanocomposites. It is worth emphasizing that molecular dynamics (MD) simulations serve as a valuable instrument when directly employed to elucidate nanoscale interactions among composite materials and to obtain qualitatively correlations between these interactions and the overarching mechanical properties observed on a macroscale [49]. However, comparing MD results with experimental findings poses a challenge due to the substantial disparity, spanning several orders of magnitude, between laboratory strain rates and those characteristic of MD simulations. Various methodologies have been devised to bridge this gap [49–51]. For instance, it is known that increases in temperature impact the elastic modulus of polymers in a manner akin to increases in strain rates. This forms the basis for the time-temperature superposition used in constructing "master curves" for polymers. These master curves establish a relation between the elastic modulus and a broad range of strain rates. MD simulations use the constant relation between experimental and simulation master curves to reasonably predict the mechanical properties of polymers at a macroscale. However, it's worth noting that such "upscale" methods are predominantly applicable to polymers due to the abundance of experimental data available compared to novel

Table 2
Structural data on PEG and nanocomposites, where H is depth (defined in y-axis), W is width (defined in x-axis), L is length (defined in z-axis), N is the total number of atoms and ρ is the density.

		H (Å)	W (Å)	L (Å)	N	ρ (g cm^{-3})
Polymer	PEG	57.0	57.0	57.0	19,990	1.13
Nanocomposite	PEG/G	57.0	57.0	57.0	20,424	1.17
	PEG/GO-1PEG-S	–	–	–	20,276	–
	PEG/GNH-1PEG-S	–	–	–	20,518	–
	PEG/GNH-2PEG-L	–	–	–	20,553	–
	PEG/GNH-1PEG-S-NH_2	–	–	–	20,422	–

nanocomposites. Consequently, these methodologies are presently beyond the scope of the current study. Uniaxial tension was applied in both longitudinal and transverse directions of the nanofillers. Young's modulus (Y) was calculated in small deformation range $0 < \varepsilon < 0.05$ (elastic). This deformation approach was first employed to pristine PEG, which permitted validation by comparing the extracted mechanical properties with those available in the literature [52–54].

3. Polymer-grafted graphene

3.1. Mechanical properties

The mechanical behaviour of polymer-grafted graphene sheets under tensile loading (positive strain, $\varepsilon > 0$) and compressive loading (negative strain, $\varepsilon < 0$) is discussed in this section. Representative tensile stress versus strain curves are shown in Fig. 4. The mechanical properties of pristine graphene and polymer-grafted graphene sheets at 100 K are shown in Table 4. The results obtained for pristine graphene are in good agreement with published results using the same potential (~1.5 TPa) [23,42].

It is known that 2D materials are usually much weaker for compression than for tension. From Fig. 4, it can be observed that tensile strengths are much higher than compressive strengths. Regardless of the loading direction (compressive or tensile loading), stress-strain curves for pristine graphene have higher slopes than those for polymer-grafted graphenes. Overall, grafting polymers in graphene sheets decreases their elastic modulus because an imperfection (graft) is introduced into the pristine sheet. Accordingly, the Young's modulus for polymer-grafted graphenes have lower values than graphene, with drops between 22% and 52%, see Table 4. With respect to tensile loading, grafting also decreases the ultimate stress (σ_{ult}) but generally increases the failure strain (ε_{cr}). In compressive loading, the presence of polymeric grafts decreases σ_{ult} and ε_{cr}, with exception in the latter for GNH-2PEG-L and GNH-1PEG-NH_2.

To understand the influence of the functional groups that bonds the polymer chain to the graphene, the mechanical properties of GNH-1PEG-S, GO-1PEG-S systems are compared. For both tensile and compressive loading the system containing the NH_2 functional group shows lower Y, lower ultimate stress, and lower failure strain, than the system containing the OH functional group, with exception of the failure stress that denotes an opposite trend. Bonding polymer chains to graphene with $–NH_2$ functional groups leads to weaker mechanical properties than bonding the same polymer chains with –OH. In the other hand, grafting longer polymer chains to graphene, or using an already functionalized graphene sheet for grafting, leads to detrimental mechanical behaviour of the grafted graphene.

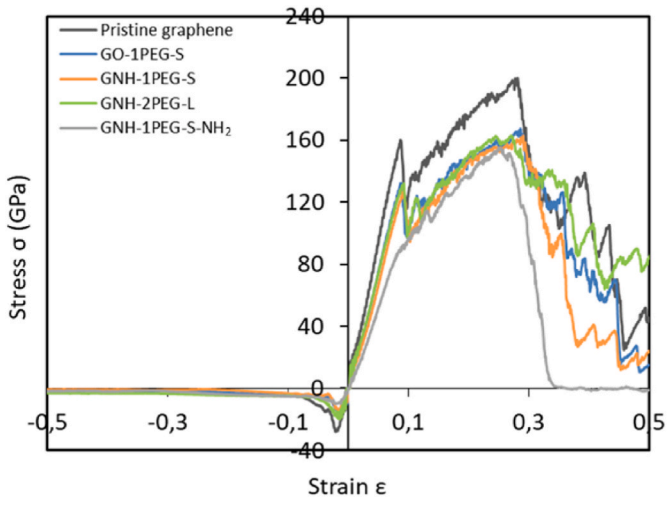

Fig. 4. Stress-strain curves of pristine graphene and PEG-grafted graphene.

ReaxFF is applied here since it is a reactive potential that can model the complete polymer-grafted graphene systems. It can model bond breaking (polymer and graphene), deformation mechanisms and rupture whereas other potentials cannot. A detailed analysis of the deformation and rupture of polymer-grafted chains and of graphene sheets is presented next. However, PEG-polymer grafted graphenes systems cannot be modelled by ReaxFF, due to excessive computer costs. In these systems, graphene sheets are modelled by a less "expensive" potential such as AIREBO in conjunction with OPLS. Stress-strain curves for polymer-grafted graphenes at 10 K, 100 K and 300 K are presented in Appendix C. The results for these systems modelled by AIREBO + OPLS shown that ReaxFF overestimates stress in tensile loadings, which is a known conclusion. It also shows how the mechanical properties of the systems degrade with temperature. Stress can also be calculated from Force divided by transversal Area. In this case, Force can be obtained from LAMMPS for the fixed atoms in both boundaries and is irrespective of the polymer chain volume. This was tested and the results are shown in Appendix D (Fig. D1 and Table D1). It can be seen that the differences are small, but the Force curves are less "smooth". Since MD simulations for the mechanical characterization of polymer-grafted graphenes are not easily available in the literature, a detailed analysis of the deformation mechanisms under tensile and compression with ReaxFF is shown next. Two systems were selected: (i) the system GNH-2PEG-L grafted with two long polymer chains under compression and (ii) the system GNH-1PEG-S grafted with one small polymer under tension.

3.2. Buckling behaviour under compression

Fig. 5 presents the variation of the compressive stress with the imposed strain of GNH-2PEG-L. Fig. 6 shows the deformed configurations of GNH-2PEG-L at points a-e displayed along the $\sigma(\varepsilon)$ curve of Fig. 5. According to the deformed configurations of the graphene sheets, the $\sigma(\varepsilon)$ curve can be divided into three stages: I – pre-buckling, II – post-buckling, III – folding.

In stage I, the compressive stress evolves linearly (proportionally) with the strain until point *a* (Fig. 6a). At point *a*, the sheet buckles in a low amplitude single-wave mode shape. From this point on (stage II), the compressive stress suddenly drops and the sheet changes directly from the low amplitude single-wave mode (Fig. 6a) to a low amplitude three-wave mode shape (Fig. 6b). After the huge drop of stress, the sheet configuration changes to a two-wave mode with moderate amplitudes (Fig. 6c). From now onward, the stress decreases smoothly with increasing strain because the buckled sheet has residual stiffness, and the sheet shifts to a single-eave mode shape (Fig. 6d). In stage III, the stress practically does not change for increasing strain but the amplitude of the single-wave mode increases highly (Fig. 6e). During the post-buckling deformation process, PEG chains grafted onto graphene follow a similar deformation as the graphene sheet. At high levels of compression, the PEG chain inside the fold tends to wrap around (Fig. 6e).

3.3. Fracture behaviour under tension

Fig. 7 shows the variation of tensile stress with the imposed strain of GNH-1PEG-S. The deformed configurations of GNH-1PEG-S at points a-d shown in the $\sigma(\varepsilon)$ curve of Fig. 7 are presented in Fig. 8. The stress increases almost linearly with the strain (up to point a). At the onset of this point, the first C–C bond fails in graphene and the stress exhibits a sudden drop. As the strain continuously increases, the sheet still shows an impressive stiffness and the stress recovers beyond that of point *a*. This rise stops at point b, which corresponds to the maximum ultimate stress σ_{ult}, where one of the C–C bonds of the PEG polymer also breaks (Fig. 8b). From this point forward, the stress sharply decreases and a series of drops characteristic of the graphene fracture occurs (Fig. 8c), until the total rupture of the sheet into two similar parts (Fig. 8d).

Table 4
Young's modulus (Y) in TPa, Ultimate stress (σ_{ult}) in GPa and failure strain (ε_f) obtained for PEG-grafted graphene. Variation percentage of systems in relation to pristine graphene is also presented.

Systems	Y	%	Tension				Compression			
			σ_{ult}	%	ε_f	%	σ_{ult}	%	ε_{cr}	%
Pristine graphene	1.86		190.59		0.239		27.97		0.021	
GO-1PEG-S	1.45	−22	167.50	−12	0.286	+20	16.62	−41	0.017	−19
GNH-1PEG-S	1.27	−32	162.89	−15	0.291	+22	14.12	−50	0.015	−29
GNH-2PEG-L	0.90	−52	130.51	−32	0.227	−5	10.22	−63	0.022	+5
GNH-1PEG-S-NH_2[a]	0.98	−47	155.16	−19	0.251	+5	9.94	−64	0.023	+10

[a] Graphene sheet functionalized with 10 % –NH_2.

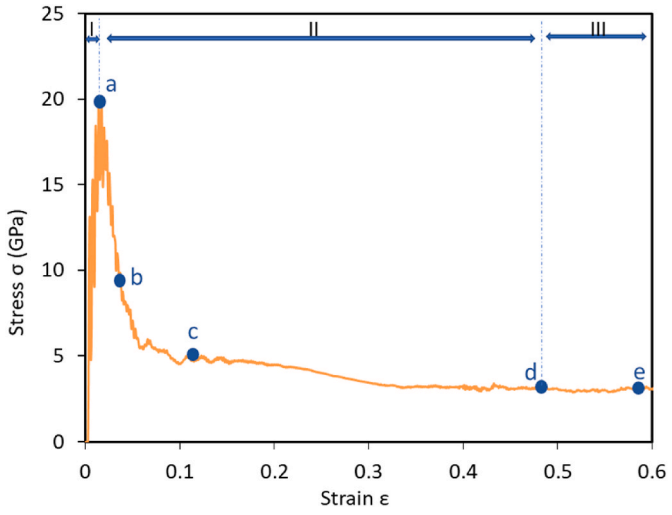

Fig. 5. Stress-strain curve of GNH-2PEG-L under compressive loading and its 3 stages (I, II, II).

4. PEG nanocomposites reinforced with PEG-grafted graphene

4.1. Mechanical properties of nanofillers and matrix

Some authors [55–57] state that polymer-grafted graphenes are efficient nanofillers in polymer composites. The amphiphilic nature of the polymer-grafted graphene is one of the causes for the improvement of mechanical properties of the polymer nanocomposite [55]. Other authors [58] found that nanoparticles grafted with matrix molecular chains improve the dispersion in the polymer matrix. Moreover, Liu et al. [23] found that grafting polymer molecular chains on graphene can improve the dispersion of the graphene in a polymer matrix. Their results showed that grafting short PE molecular chains on graphene significantly improve the interfacial shear strength and interfacial fracture toughness of functionalized graphene/PE nanocomposites. Thus, in second part of this paper, the mechanical properties of a PEG matrix reinforced with GO-1PEG-S, GNH-1PEG-S, GNH-2PEG-L,

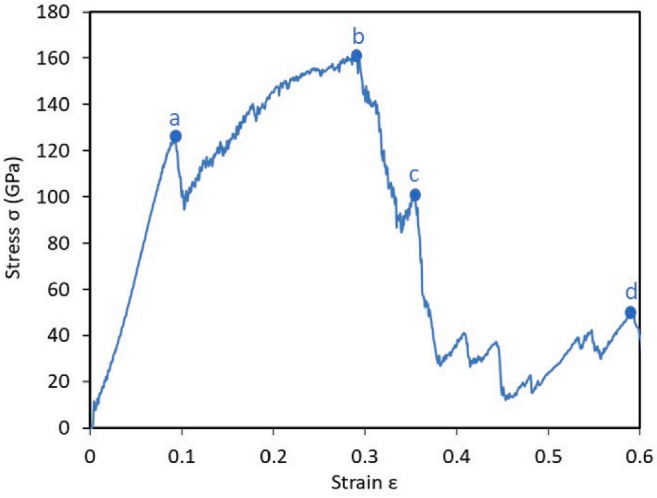

Fig. 7. Stress-strain of GNH-1PEG-S under tensile loading.

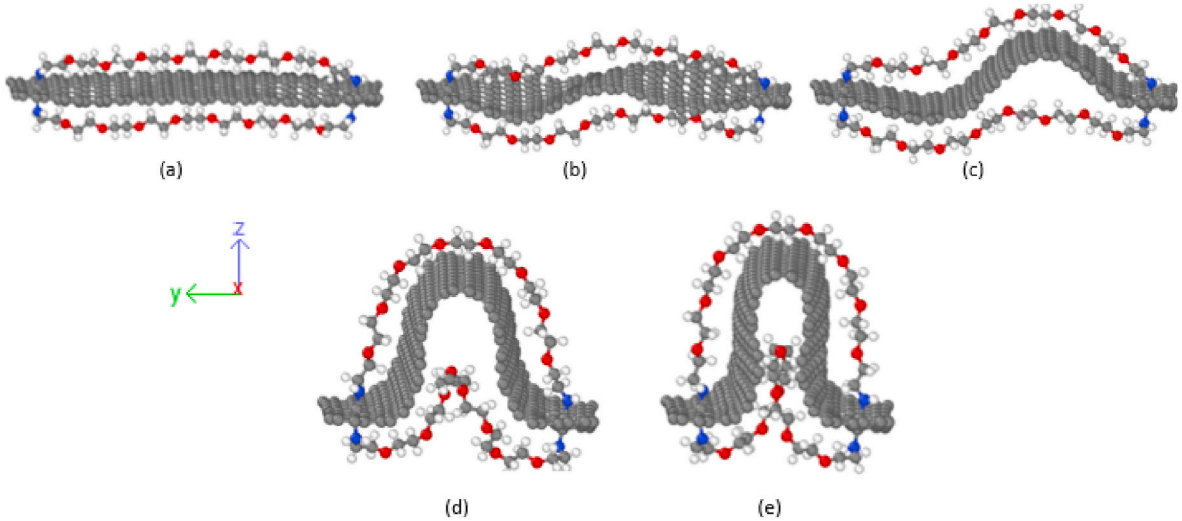

Fig. 6. Deformed configurations of the GNH-2PEG-L at points a-e shown in σ(ε) curve of Fig. 5: (a) ε = 0.014 (σ_{ult}), (b) ε = 0.037, (c) ε = 0.118, (d) ε = 0.493, (e) ε = 0.599.

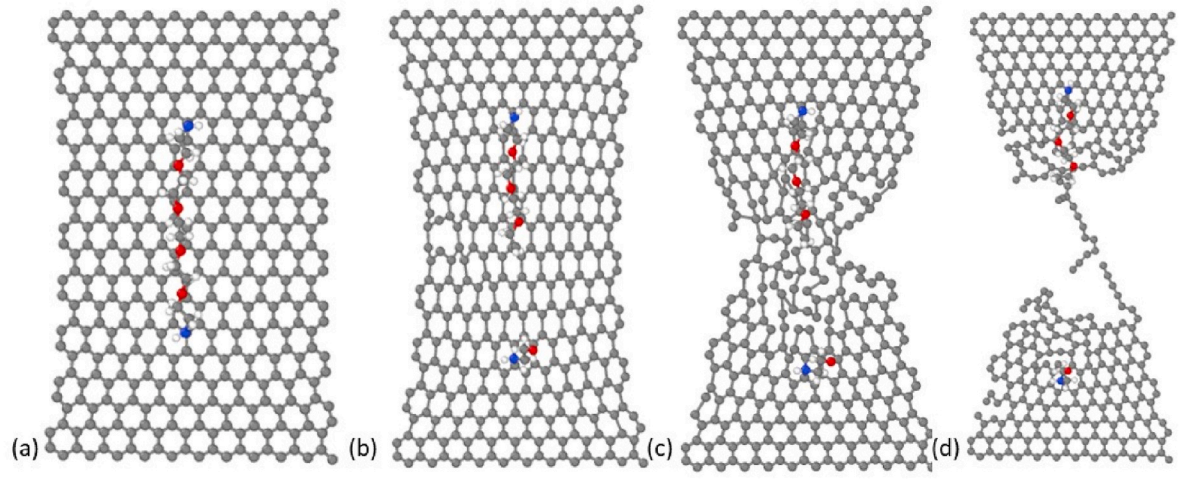

Fig. 8. Configurations of the GNH-1PEG-S at points a-e shown in σ(ε) curve of Fig. 7. (a) ε = 0.092, (b) ε = 0.291 (σ_{ult}), (c) ε = 0.350, (d) ε = 0.594.

GNH-1PEG-S-NH_2 are investigated, giving rise to the following nanocomposites: PEG/GNH-1PEG-S, PEG/GNH-2PEG-L, PEG/GNH-1-PEG-S-NH_2, PEG/GO-1PEG-S. For comparative purposes, the reference PEG/G nanocomposite is also analysed.

The ReaxFF force field has been used in previous simulations. It is known that this potential can model accurately bond breaking and the formation of new bonds for mechanical loadings in graphene-based materials, particularly systems that include other atomic elements besides carbon, most notably N and O, which AIREBO alone, for example, cannot model accurately. However, when applied to larger systems (systems with higher number of atoms) ReaxFF leads to a huge computational time (50 times slower [59] than other more "light" potentials, such as AIREBO and OPLS-AA), mainly due to its explicit modelling of bond formation and breaking, the dynamic charge equilibration at each timestep, and its one order smaller timestep. All these parameters pose significant computational challenges in simulation capability to reach spatial-temporal scales of nanometres and nanoseconds [28,59]. Therefore, two potentials commonly applied to simulate graphene reinforced polymer nanocomposites were chosen [60–63]: AIREBO and OPLS-AA. To assess their validity, these two potentials were applied to the simulation of the two "most simple" systems: GNH-1PEG-S and GO-1PEG-S. The stress-strain curves are represented in Appendix A. The Y values obtained for GNH-1PEG-S and GO-1PEG-S are presented in Table 5. Expectedly, these values are lower than those obtained by the ReaxFF forcefield, because ReaxFF overestimates the stress values [64].

Now let us look at the mechanical behaviour of the polymeric matrix PEG, and its properties along the x, y and z directions. This analysis was performed for all loading directions to assess the inhomogeneity and isotropy of PEG. A temperature of 100 K wa used for all simulations, which is below the glass transition temperature and the melting temperature [65,66]. Fig. 9 presents the stress-strain curve for PEG, along x, y and z direction, at a temperature of 100 K and a strain rate of 10^{10} s^{-1}. The shape of the curve is qualitatively similar along the three directions, however, when the deformation is imposed in z direction, the stress values are slightly lower (grey line) than in the other directions (orange and blue lines). The stress-strain curves show four different regions: elastic, yielding, softening and hardening. In the elastic region, the stress increases linearly (proportionally) with the strain. At the molecular level, the linear elastic behaviour is caused by van der Waals (vdW) forces acting between the PEG polymer chains. When the strain reaches a critical level, the vdW forces achieve their peak and after that they decrease, leading the polymer chains to sliding between them. Then, the yielding deformation begins, meaning the stress does not change much (small fluctuations) for increasing strains. The yield point indicates the local maximum stress value of the material. Beyond yielding, the polymer chains adapt and accommodate to each other and the stress decreases to a minimum, indicating softening of the material. After the chains have been accommodated in a new arrangement, the stresses start rising again due to strain hardening. The strain hardening is a result of the randomly oriented polymer chains re-aligning themselves in such a way that it requires the application of a higher force for increased deformation. The PEG mechanical properties for the three directions are shown in Table 6. In case of the, The highest value Young's modulus Y was obtained for the x direction. While y direction shows The highest value of yield stress σ_y was obtained for the y direction. The Z direction shows lower values of Y and σ_y. Although it is a cubic box in which the polymer chains are randomly placed inside the simulation box, these differences are due to the orientation of the polymer chains in the matrix, which is not homogeneous and truly isotropic at nanoscale.

Table 5
Comparison of Young's modulus Y (TPa) between ReaxFF and AIREBO potentials.

	ReaxFF	AIREBO
GNH-1PEG-S	1.27	0.58
GO-1PEG-S	1.45	0.64

From the previous results, it can be concluded that the extracted mechanical properties are in the range of experimental/theoretical values previously published (Y between 0.98 and 6.5 GPa) [52–54]. This means that the model may accurately simulate the tensile test of the systems.

4.2. Mechanical behaviour of PEG-grafted graphene composites

This section presents the main results on the mechanical characterization of PEG-grafted graphene composites. For illustration purposes, Fig. 10 shows the equilibrated structure of PEG/GNH-2PEG-L at 300 K (prior to the deformation process). The structures of the remaining PEG/nanofiller systems as well as the polymer matrix are also presented in Appendix B. The configuration of polymer shows an amorphous structure with randomly entangled chains.

To analyse the effects induced by the graphene reinforcements, the values of the radius distribution function (g(*r*)) that describes the distribution of the relative distances between the PEG matrix atoms and the nanofiller atoms are shown in Fig. 11. It can be seen that the nanocomposites reinforced with PEG-grafted graphene (PEG/GNH-1PEG-S, PEG/GNH-2PEG-L, PEG/GNH-1PEG-NH_2, PEG/GO-1PEG-S) show much higher g(*r*) values than the pristine graphene-reinforced nanocomposite (PEG/G). This indicates that there is a greater number of polymer chains

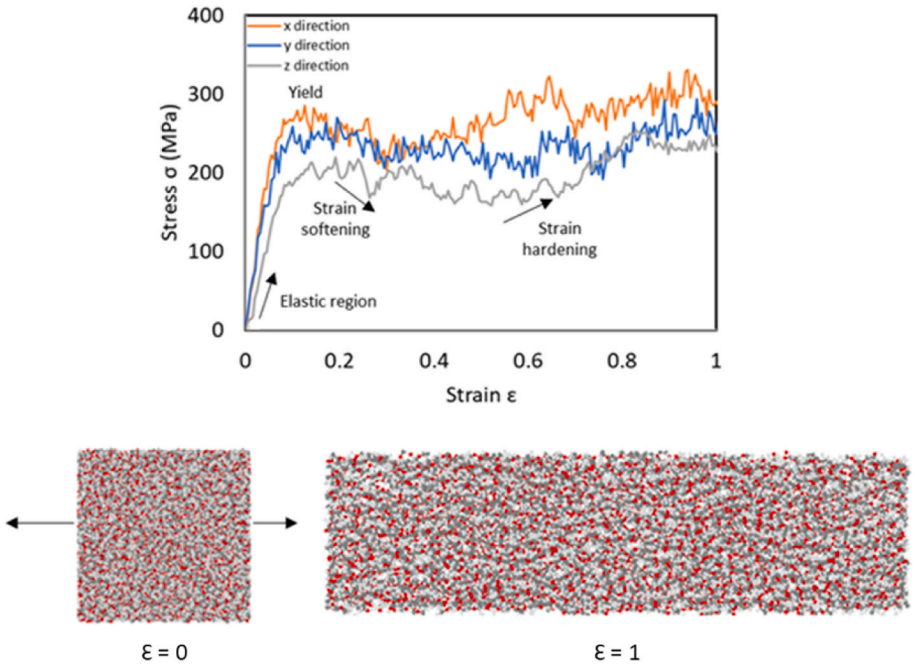

Fig. 9. Stress-strain response of PEG deformed in uniaxial tension at strain rate of 10^{10} s^{-1} and temperature of 100 K, at different loading directions. The snapshots correspond to the stress-strain curve along the x-axis.

Table 6
Young's modulus (Y), yield stress (σ_y) of PEG at different loading directions.

Loading direction	Y (GPa)	σ_y (MPa)
x	4.32	285.40
y	3.73	270.19
z	2.24	212.77

gathered around the PEG-grafted graphenes than around the pristine graphene. This is due to the more compact interfacial space and the higher interactive strength between the nanofiller and the polymer matrix [67]. Of the four PEG-grafted graphene nanocomposites, PEG/GNH-1PEG-S-NH_2 shows higher g(r) values (grey curve), since there is also interaction between the functional groups (-NH_2) of the nanofiller and the polymer matrix.

To further explore the enhanced effects induced by polymer-grafted graphene reinforcements, the average values of the interfacial interaction energy between different types of nanofiller and PEG matrix are also analysed. As shown in Fig. 12, it can be deduced that the functionalization of the graphene sheet increases the magnitude of the interaction energy. Grafting small polymer chains on graphene promotes a positive interaction between grafted sheets and the bulk polymer because non-bonding forces increase. This is translated in a higher adhesion between the graphene surface and PEG matrix. The negative values of the interaction energy denote the presence of attractive interaction between the PEG-grafted graphene and PEG matrix [68]. On the contrary, slightly positive values for bare graphene shows no interaction to slightly repulsive interaction between the two materials. These results agree well with the analysis of g(r) previously shown in Fig. 11.

Next, the tensile mechanical behaviour in both the longitudinal and

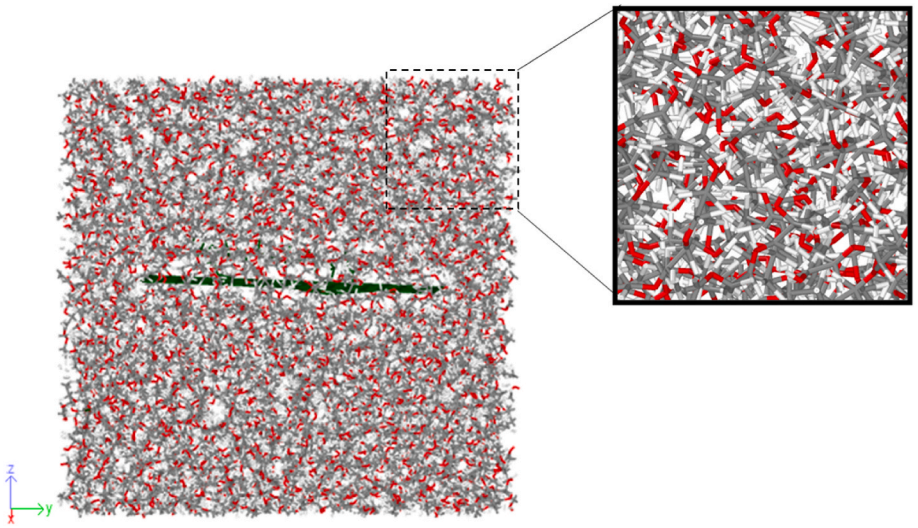

Fig. 10. Representation of PEG/GNH-1PEG-S prior to the deformation process. The grey, red, and white colours represent the carbon, oxygen, and hydrogen atoms, respectively. The green colour represents the nanofiller.

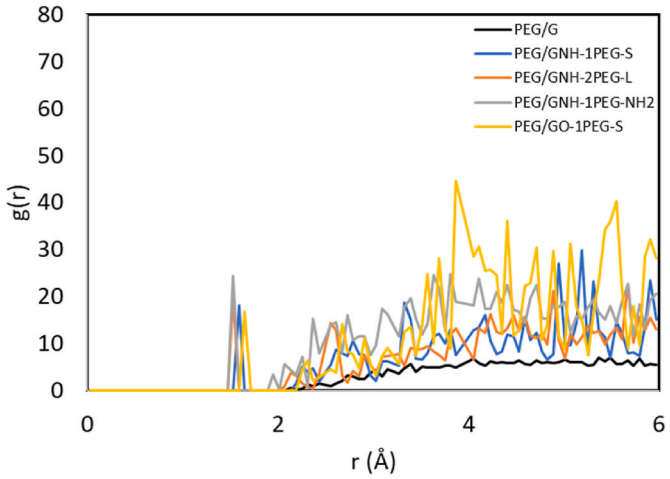

Fig. 11. Radial distribution functions for PEG nanocomposites before deformation process.

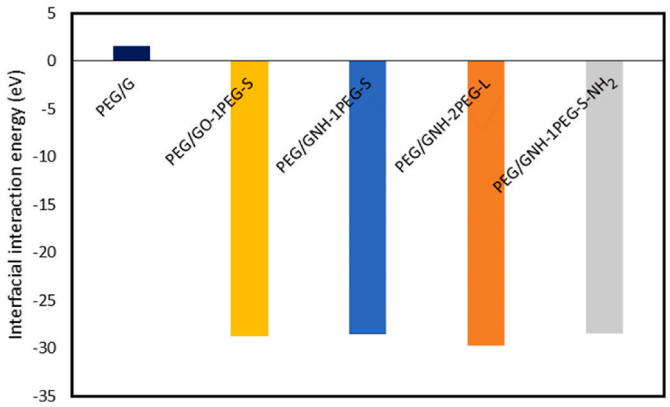

Fig. 12. Variation of the interfacial interaction energy between different nanofillers and PEG matrix before deformation process.

transversal directions of the nanofillers is presented. The mechanical properties obtained for pure PEG and the nanocomposites are presented in Table 7 and the stress-strain curves are given in Fig. 13.

The mechanical properties of the nanocomposites are greatly improved by the PEG-grafted graphene when the deformation is imposed along the length of the graphene sheet. Along transversal direction, only the GNH-2PEG-L nanofiller increases the values of Y and σ_y by 13 %. When the deformation is imposed along longitudinal direction, The presence of some nanofillers (Graphene, GNH-1PEG-S and GNH-2PEG-L) in the polymer matrix significantly increases (by 23–43 % in relation to PEG) the value of Y for the transversal direction, particularly the GNH-1PEG-S, which increases Y by 43 % and σ_y by 31 %.

Both PEG/GNH-1PEG-S and PEG/GO-1PEG-S nanocomposites are visually quite similar, differing only the group bonding PEG polymer chain to graphene in the nanofiller. In PEG/GNH-1-PEG-S nanocomposite the group connecting the polymer chain to graphene is a $–NH_2$ group while in PEG/GO-1PEG-S nanocomposite the group connecting the PEG chain to graphene is a –OH group. However, they possess completely distinct mechanical properties when embedded in the polymer matrix. When loaded in the longitudinal direction, the GNH-1PEG-S nanofiller significantly increases the Y of PEG, in contrast to GO-1PEG-S, which basically does not change the Y value. In the transversal direction, the PEG/GO-1PEG-S nanocomposite also shows rather poor mechanical properties when compared to PEG/GNH-1PEG-S. Fig. 14 illustrates the behaviour of PEG/GNH-1PEG-S, PEG/GNH-1PEG-S-NH_2 and PEG/GO-1PEG-S nanocomposites at $\varepsilon = 1$ along the longitudinal direction. By observing the behaviour of PEG/GNH-1PEG-S and PEG/GO-1PEG-S nanocomposites during the deformation process along longitudinal direction (Fig. 14a) and c)), it can be seen that there is rupture of the graphene sheet in PEG/GO-1PEG-S nanocomposite. Conversely, the PEG/GNH-1PEG-S nanocomposite only exhibits the alignment of the polymer chains of the PEG matrix along the loading direction. This event could explain the divergence between the mechanical properties obtained in the two nanocomposites.

The functionalization of the graphene sheet (GNH-1PEG-S-NH_2) does not provide benefits to the PEG/nanofiller system in longitudinal direction because by comparing the same system with and without functionalization of the nanofiller (PEG/GNH-1PEG-S-NH_2 and PEG/GNH-1PEG-S, respectively), the former hardly changes the value of Y for pure PEG, while the latter increases the value of Y by 43 %. Regarding transversal direction, the results obtained for these two nanocomposites are quite similar. Although in both nanocomposites the interaction between the nanofiller and the PEG matrix is high, the intrinsic properties of the nanofiller differ, namely the Young's modulus Y. The value of Y is higher for GNH-1PEG-S (1.27 TPa) than for GNH-1PEG-S-NH_2 (0.98 TPa), due to the improved mechanical properties of the nanocomposite along the nanofiller direction. Like PEG/GO-1PEG-S, the graphene sheet rupture (Fig. 14b)) is also observed in the case of PEG/GNH-1PEG-S-NH_2, which also deteriorates the mechanical properties of the nanocomposite.

Finally, it is known that the rule of mixtures is widely used to predict the elastic properties of composite materials. Based on the weighted contributions of the filler and matrix, and assuming that the strain of nanofiller is equal to that of polymer matrix [69,70], the Young's modulus of the nanocomposite Y may be estimated by

$$Y = \left[f_f/Y_n + (1 - f_f)/Y_m\right]^{-1} \quad (1)$$

where the subscript n represents the *nanofiller* and m denotes the *matrix (PEG)*, f_f is the fraction of the nanofiller, Y_n and Y_m are the Young's modulus of the nanofiller and matrix, respectively. Two type of fraction f_n are presented: (i) the standard volume fraction of the nanofiller (f_{nv}) and the atomic fraction of the nanofiller (f_{na}), which is based on the number of atoms. The results obtained are shown in Table 8 for the longitudinal direction and Table 9 for the transversal direction. It is found that the volume fraction f_{nv} is comparable to the atomic fraction f_{na} (the ratio f_{nv}/f_{na}, ranges between 0.72 and 1.22 in both directions). The values of Y given by the rule of mixtures provided a good prediction of Y obtained from MD simulations, using either f_{nv} or f_{na}. In the case of

Table 7
Young's modulus Y (GPa) and yield stress σ_y (MPa) of PEG and PEG nanocomposites for the longitudinal and transversal directions.

Nanocomposite	Longitudinal direction				Transversal direction			
	Y	%	σ_y	%	Y	%	σ_y	%
PEG	3.73	–	270.19	–	4.32	–	285.40	–
PEG/G	4.59	+23	284.15	+5	4.21	0	286.96	+1
PEG/GNH-1PEG-S	5.33	+43	354.60	+31	4.43	+3	297.53	+4
PEG/GNH-2PEG-L	4.84	+30	330.40	+22	4.88	+13	323.92	+13
PEG/GNH-1PEG-S-NH_2	3.68	−1	259.95	−4	4.42	+2	298.89	+5
PEG/GO-1PEG-S	3.84	+3	254.51	−6	3.45	−20	241.77	−15

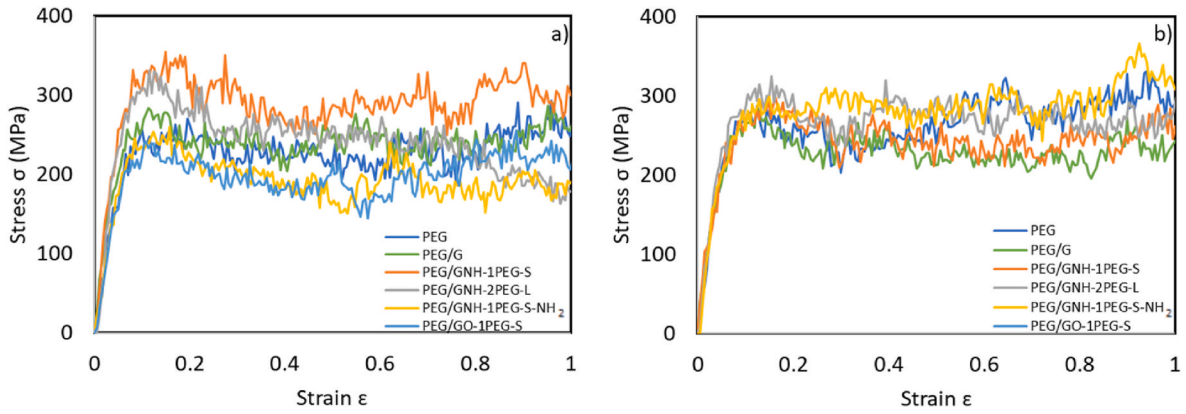

Fig. 13. Stress-strain curves of PEG and PEG-nanocomposites at different loading directions: (a) longitudinal direction and (b) transverse direction.

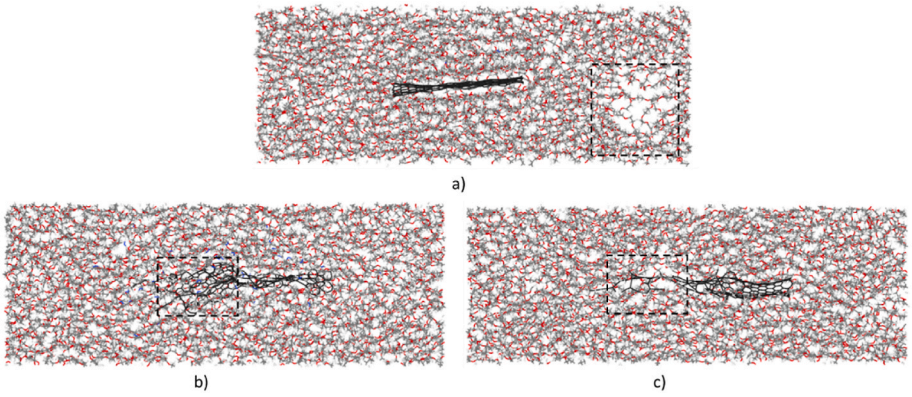

Fig. 14. Illustrations of (a) PEG/GNH-1PEG-S, (b) PEG/GNH-1PEG-S-NH_2, c) PEG/GO-1PEG-S at ε = 1, along longitudinal direction. The PEG-nanocomposites structure has been cut to show the embedded nanofillers. C atoms of graphene are coloured dark grey, C atoms of PEG matrix are coloured grey, O atoms are coloured red, H atoms are coloured white and N atoms are coloured blue.

Table 8
Comparison between the Young's modulus Y of nanocomposites for the *longitudinal* direction, computed from MD and predicted from rule of mixtures. The Young's modulus of PEG matrix and nanofillers, computed from MD, are $Y_m = 3.73$ GPa in longitudinal direction and $Y_m = 4.32$ GPa in transverse direction, $Y_n = 1.86$ TPa (Graphene), $Y_n = 1.27$ TPa (GNH-1PEG-S), $Y_n = 1.47$ TPa (GNH-2PEG-L), $Y_n = 0.98$ TPa (GNH-1PEG-S-NH_2), and $Y_n = 1.45$ TPa (GO-1PEG-S).

Nanocomposite	Y (1)	Volume fraction			Atomic fraction		
		f_{nv} (%)	Y (2)	(2)/(1)	f_{na} (%)	Y (3)	(3)/(1)
PEG/G	4.59	1.78	3.80	0.83	1.94	3.80	0.83
PEG/GNH-1PEG-S	5.33	1.85	3.80	0.71	2.57	3.83	0.72
PEG/GNH-2PEG-L	4.84	2.13	3.81	0.79	1.75	3.80	0.78
PEG/GNH-1PEG-S-NH_2	3.68	2.04	3.81	1.03	2.76	3.84	1.04
PEG/GO-1PEG-S	3.84	2.04	3.81	0.99	2.13	3.81	0.99
			Avg	0.87		Avg	0.87

Table 9
Comparison between the Young's modulus Y of nanocomposites for the *transversal* direction, computed from MD and predicted from rule of mixtures. The Young's modulus of PEG matrix and nanofillers, computed from MD, are $Y_m = 3.73$ GPa in longitudinal direction and $Y_m = 4.32$ GPa in transverse direction, $Y_n = 1.86$ TPa (Graphene), $Y_n = 1.27$ TPa (GNH-1PEG-S), $Y_n = 1.47$ TPa (GNH-2PEG-L), $Y_n = 0.98$ TPa (GNH-1PEG-S-NH_2), and $Y_n = 1.45$ TPa (GO-1PEG-S).

Nanocomposite	Y (1)	Volume fraction			Atomic fraction		
		f_{nv} (%)	Y (2)	(2)/(1)	f_{na} (%)	Y (3)	(3)/(1)
PEG/G	4.34	1.78	4.40	1.01	1.94	4.41	1.02
PEG/GNH-1PEG-S	4.43	1.85	4.40	0.99	2.57	4.43	1.00
PEG/GNH-2PEG-L	4.88	2.13	4.41	0.90	1.75	4.40	0.90
PEG/GNH-1PEG-S-NH_2	4.42	2.04	4.41	1.00	2.76	4.44	1.00
PEG/GO-1PEG-S	3.45	2.04	4.41	1.28	2.13	4.41	1.28
			Avg	1.04		Avg	1.07

f_{nv} (nanofiller volume fraction), the difference ranges between −1.53 % and +0.13 % in longitudinal direction and between −0.47 % and +0.96 % in transversal direction. In the case of f_{na} (nanofiller atomic fraction), the difference varies between −1.50 % and +0.16 % in longitudinal direction and between −0.48 % and +0.96 % in the transverse direction.

5. Conclusion

The mechanical behaviour of PEG nanocomposites with graphene grafted with polymer chains under tensile loading and compressive loading was studied using molecular dynamics. Stress-strain curves were obtained, and mechanical properties were extracted. First, the influence of the functional groups (-NH_2 and –OH) that bond the polymer chain to graphene was analysed. It was found that the system containing the –NH_2 functional group showed lower mechanical properties than the system containing the –OH functional group. The 10 % functionalization of graphene sheet showed no advantages over the sheet without functionalization. The deformation mechanisms under compression and tension were observed. The stress-strain curve for compression clearly exhibited three phases: elastic compression, buckling and folding. The stress-strain curve for tension showed two distinct parts (PEG polymer rupture and sheet rupture).

The mechanical properties of five PEG-nanocomposites were investigated: PEG/G, PEG/GNH-1PEG-S, PEG/GNH-2PEG-L, PEG/GNH-1PEG-S-NH_2, PEG/GO-1PEG-S. The radius distribution function values and the variation of interfacial interaction energy were also examined. The radius distribution function values indicated a larger number of polymer chains gathered around the polymer graphene than the pristine graphene. Functionalization of the graphene sheet also increased the magnitude of the interaction energy, also revealing greater adhesion between graphene surface and PEG matrix. The effect of nanofillers on the mechanical properties of the nanocomposites in longitudinal direction and in transverse direction was also analysed. It was found that the mechanical properties of PEG were mostly improved in the longitudinal direction (reinforcement up to 43 %). It was also seen that functionalization of the graphene sheet had no benefits for the PEG/nanofiller system. Despite the high interaction between the nanofiller and PEG matrix, the low intrinsic properties of the nanofiller, namely Young's modulus, as well as the rupture of the graphene sheet during the deformation process deteriorated the mechanical properties of the nanocomposite. Finally, the rule of mixtures provided a good prediction of Young's modulus in the directions longitudinal and transverse for both volume fraction and atomic fraction estimates.

CRediT authorship contribution statement

Cátia Guarda: Writing – original draft, Visualization, Software, Methodology, Investigation, Formal analysis, Data curation. **Bruno Faria:** Writing – original draft, Visualization, Software, Methodology, Investigation, Formal analysis, Data curation, Conceptualization. **José N. Canongia Lopes:** Supervision, Methodology, Funding acquisition, Conceptualization. **Nuno Silvestre:** Writing – review & editing, Validation, Supervision, Methodology, Funding acquisition, Conceptualization.

Declaration of competing interest

The authors declare that they have no known competing financial interests or personal relationships that could have appeared to influence the work reported in this paper.

Data availability

No data was used for the research described in the article.

Acknowledgements

This work was supported by FCT, through IDMEC, under LAETA, project UIDB/50022/2020 [Grant No. 10.54499/UIDB/50022/2020], through Centro de Química Estrutural (CQE), project UIDB/00100/2020 and through Institute for Polymers and Composites, and through IDMEC, under LAETA, project UIDP/50022/2020 [Grant No. 10.54499/UIDP/50022/2020]. The first author gratefully acknowledges the financial support given by FCT in the context of the PhD scholarship SFRH/BD/129589/2017. The second author gratefully acknowledges the financial support given by FCT in the context of the Postdoctoral contract CEECINST/00156/2018.

Appendix A

The effect of different strain rates on the mechanical properties of selected cases for polymer-grafted graphenes (Fig. A1 and Table A1) and PEG nanocomposite (Fig. A2 and Table A2).

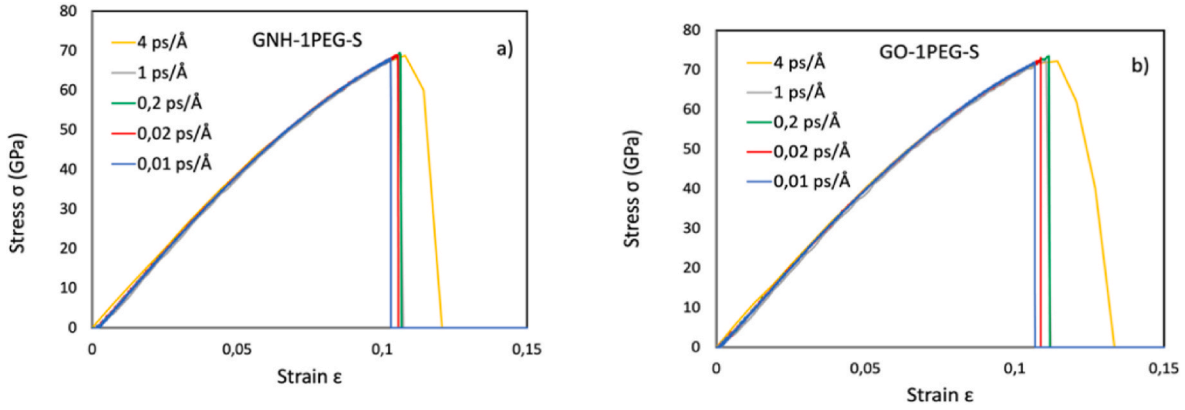

Fig. A1. Stress-strain curves of a) GNH-1PEG-S and b) GO-1PEG-S, using different strain rates: (4 ps/Å = 1,04 × 10^{11} s^{-1}; 1 ps/Å = 2,67 × 10^{10} s^{-1}; 0,2 ps/Å = 5,30 × 10^{9} s^{-1}; 0,02 ps/Å = 5,30 × 10^{8} s^{-1} and 0,01 ps/Å = 2,67 × 10^{8} s^{-1}.

Table A1
Comparison between the mechanical properties obtained for GNH-1PEG-S and GO-1PEG-S at different strain rates at 100K.

Strain rates	GNH-1PEG-S			GO-1PEG-S		
	Y	σ_{ult}	ε_f	Y	σ_{ult}	ε_{cr}
$1{,}04 \times 10^{11}\ s^{-1}$	798,1	68,76	0,109	780,7	72,2	0,120
$2{,}67 \times 10^{10}\ s^{-1}$	810,1	68,82	0,105	830,0	72,4	0,114
$5{,}30 \times 10^{9}\ s^{-1}$	814,9	69,05	0,106	810,3	73,5	0,110
$5{,}30 \times 10^{8}\ s^{-1}$	831,3	68,9	0,105	825,3	72,6	0,108
$2{,}67 \times 10^{8}\ s^{-1}$	824,3	68,1	0,103	838,8	71,9	0,106

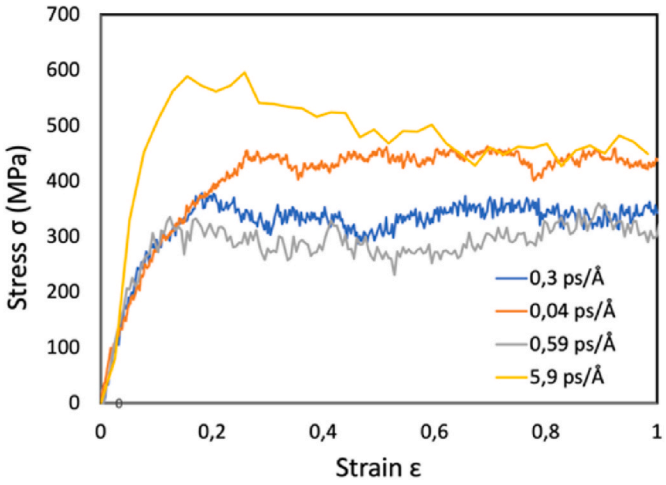

Fig. A2. Stress-strain curves of PEG-graphene using different strain rates: (5,9 ps/Å = $1{,}04 \times 10^{11}\ s^{-1}$; 0,59 ps/Å = $1{,}04 \times 10^{10}\ s^{-1}$; 0,3 ps/Å = $5{,}30 \times 10^{9}\ s^{-1}$ and 0,04 ps/Å = $7{,}02 \times 10^{8}\ s^{-1}$.

Table A2
Comparison between the mechanical properties obtained for PEG-graphene nanocomposite at different strain rates at 100K.

Strain rates	GNH-1PEG-S		
	Y	σ_{ult} (MPa)	ε_f
$1{,}04 \times 10^{11}\ s^{-1}$	6,21	588,9	0,155
$1{,}04 \times 10^{10}\ s^{-1}$	4,56	288,5	0,098
$5{,}30 \times 10^{9}\ s^{-1}$	4,20	372,6	0,178
$7{,}02 \times 10^{8}\ s^{-1}$	3,10	440,9	0,268

Appendix B

This appendix briefly shows the stress-strain curves obtained for two polymer-grafted graphene PEG (GNH-1PEG-S and for GO-1PEG-S) using different force fields at 100 K.

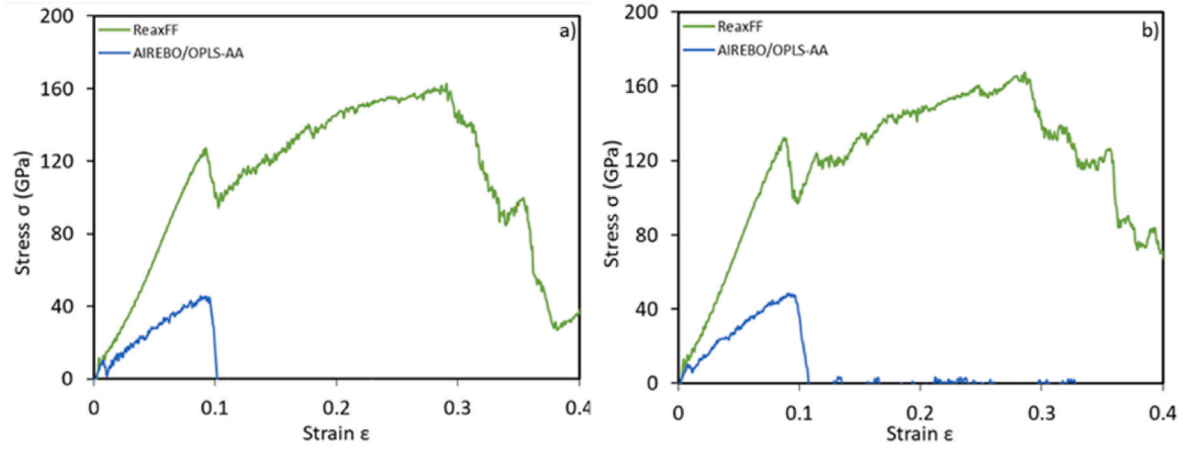

Fig. B1. Stress-strain curves of a) GNH-1PEG-S and b) GO-1PEG-S, using the $ReaxFF_{cho}$ [71] forcefield (green); AIREBO + OPLSAA [41] forcefield (blue).

Appendix C

In this appendix it is presented stress-strain curves for polymer-grafted graphenes using AIREBO + OPLS forcefield i) using volume calculation with voronoi method and using normal method and ii) at different temperatures. The mechanical properties of these graphenes are also shown in Table C1.

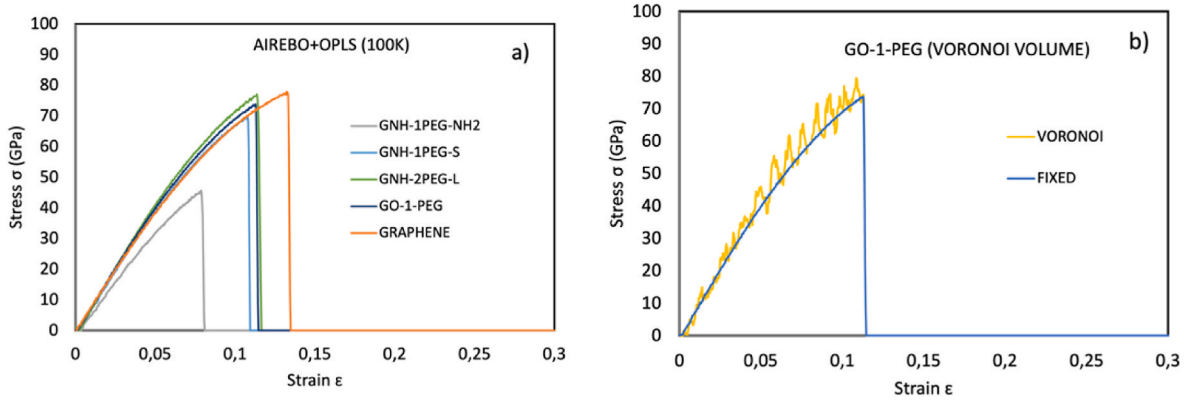

Fig. C1. Stress-strain curves of a) all the studied polymer-grafted graphene sheets and graphene using AIREBO-OPLS forcefield at 100K and b) GO-1PEG-S, also at 100K and using AIREBO-OPLS forcefield but using usual volume method (fixed graphene thickness, explained in main text) and comparing it to Voronoi volume method (volume is calculated using Voronoi tessellation).

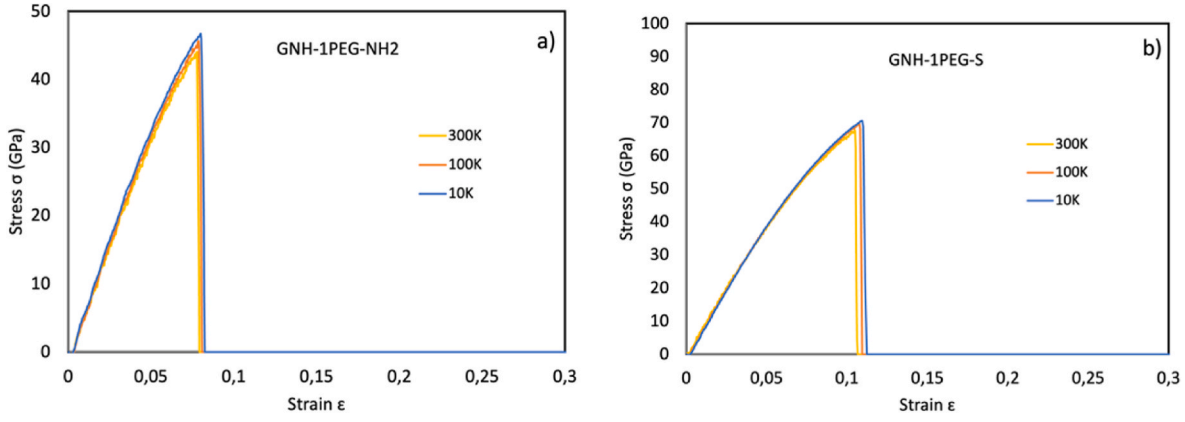

Fig. C2. Stress-strain curves at 10K; 100K and 300K of a) GNH-1PEG-NH2 and b) GNH-1PEG-S.

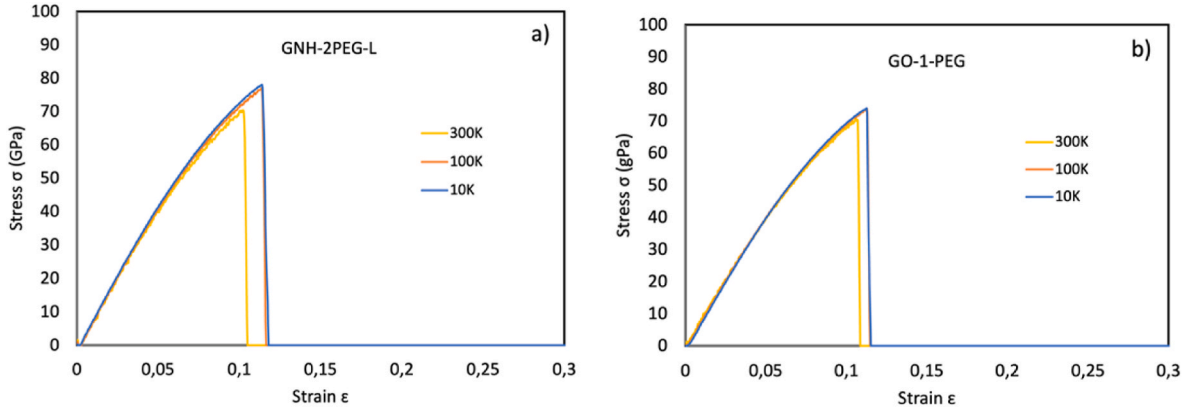

Fig. C3. Stress-strain curves at 10K; 100K and 300K of a) GNH-2PEG-L and b) GO-1PEG-S.

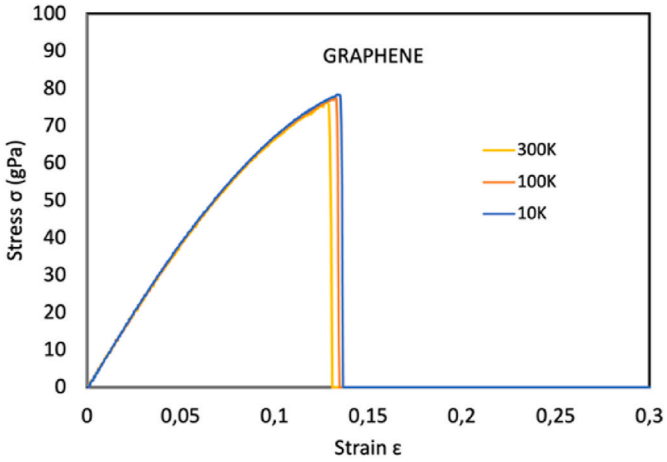

Fig. C4. Stress-strain curves at 10K; 100K and 300K of graphene sheet.

Table C1
Young's modulus (Y) in GPa, Ultimate stress (σ_{ult}) in GPa and failure strain (ε_f) obtained for PEG-grafted graphene at **10K**. Variation percentage of systems in relation to pristine graphene is also presented.

Systems	Tension					
	Y	%	σ_{ult}	%	ε_f	%
Pristine graphene	789,6	–	78,4	–	0,133	–
GNH-1PEG-S	816,5	+3,4	70,50	−10,1	0,109	−18,0
GNH-2PEG-L	871,0	+10,3	78,03	−0,5	0,113	−15,0
GNH-1PEG-S-NH2	591,2	−25,1	46,70	−40,4	0,095	−28,6
GO-1PEG-S	831,0	+5,2	74,07	−5,5	0,1122	−15,6

Table C2
Young's modulus (Y) in GPa, Ultimate stress (σ_{ult}) in GPa and failure strain (ε_f) obtained for PEG-grafted graphene at **100K**. Variation percentage of systems in relation to behaviour at 10K is presented.

Systems	Tension					
	Y	%	σ_{ult}	%	ε_f	%
Pristine graphene	782,5	−0,9	77,70	−0,9	0,131	−1,5
GNH-1PEG-S	809,6	−0,8	69,74	−1,1	0,107	−1,8
GNH-2PEG-L	870,1	−0,1	77,03	−1,3	0,113	−0,2
GNH-1PEG-S-NH2	583,4	−1,3	45,61	−2,3	0,0939	−1,2
GO-1PEG-S	823,8	−0,9	73,60	−0,6	0,1122	0,0

Table C3
Young's modulus (Y) in GPa, Ultimate stress (σ_{ult}) in GPa and failure strain (ε_f) obtained for PEG-grafted graphene at **300K**. Variation percentage of systems in relation to behaviour at 10K is presented.

Systems	Tension					
	Y	%	σ_{ult}	%	ε_f	%
Pristine graphene	771,2	−2,3	76,10	−2,9	0,127	−4,5
GNH-1PEG-S	795,7	−2,5	67,50	−4,3	0,104	−4,6
GNH-2PEG-L	851,4	−2,3	70,46	−9,7	0,102	−9,7
GNH-1PEG-S-NH2	560,98	−5,1	44,04	−5,7	0,093	−2,3
GO-1PEG-S	801,7	−3,5	70,40	−5,0	0,106	−5,5

Table C4
Young's modulus (Y) in GPa, Ultimate stress (σ_{ult}) in GPa and failure strain (ε_f) obtained for GO-PEG-S using Voronoi method for determining volume and comparison to properties using the usual method for determining volume, explained in the main text) at **10K**.

	Voronoi vol	Fixed vol	%
Y	855,0	831,0	+2,9
σ_{ult}	79,42	74,7	+7,2
ε_f	0,112	0,112	0,0

Appendix D

In this appendix it is presented Force-strain curves for polymer-grafted graphenes using AIREBO + OPLS forcefield. Force is obtained from LAMMPS calculation of atomic force at fixed atoms at the sheet boundaries, therefore irrespective of polymer chain volume. Stress is then calculated from the transversal area of the sheet, also irrespective of polymer chain volume.

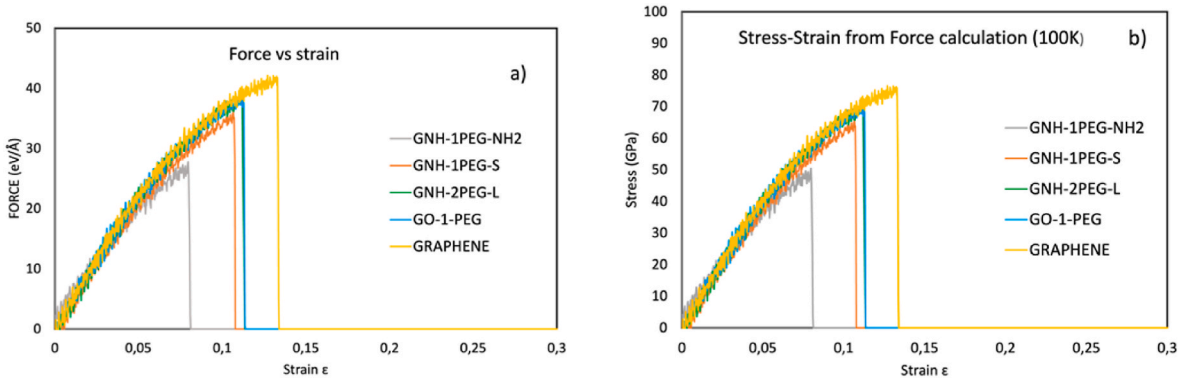

Fig. D1. a) Force-strain curves for all the studied polymer-grafted graphene sheets and graphene using AIREBO-OPLS forcefield at 100K and b) Stress-strain curves where stress is calculated from obtained Force divided by transversal sheet area.

Table D1
Young's modulus (Y) in GPa, Ultimate stress (σ_{ult}) in GPa and failure strain (ε_f) obtained for all polymer grafted graphene sheets obtained from LAMMPS stress calculation (normal method, NM, see main text) and from stress obtained from force divided by transversal sheet area (FM).

Systems	Tension						
	Y_{NM}	Y_{FM}	%	$\sigma_{ult(NM)}$	$\sigma_{ult(FM)}$	%	ε_f
Pristine graphene	789,6	828,3	+4,9	78,4	76,3	−2,7	0,133
GNH-1PEG-S	816,5	810,5	−0,7	78,1	68,9	−11,7	0,109
GNH-2PEG-L	871,0	842,6	−3,3	70,5	65,5	−7,1	0,113
GNH-1PEG-S-NH2	591,2	674,3	+14,1	45,6	50,5	+10,6	0,095
GO-1PEG-S	831,0	825,8	−0,6	74,1	70,5	−4,8	0,112

Appendix E

This appendix briefly shows the structure of the nanocomposites after equilibration and the stress-strain curves obtained during tension tests.

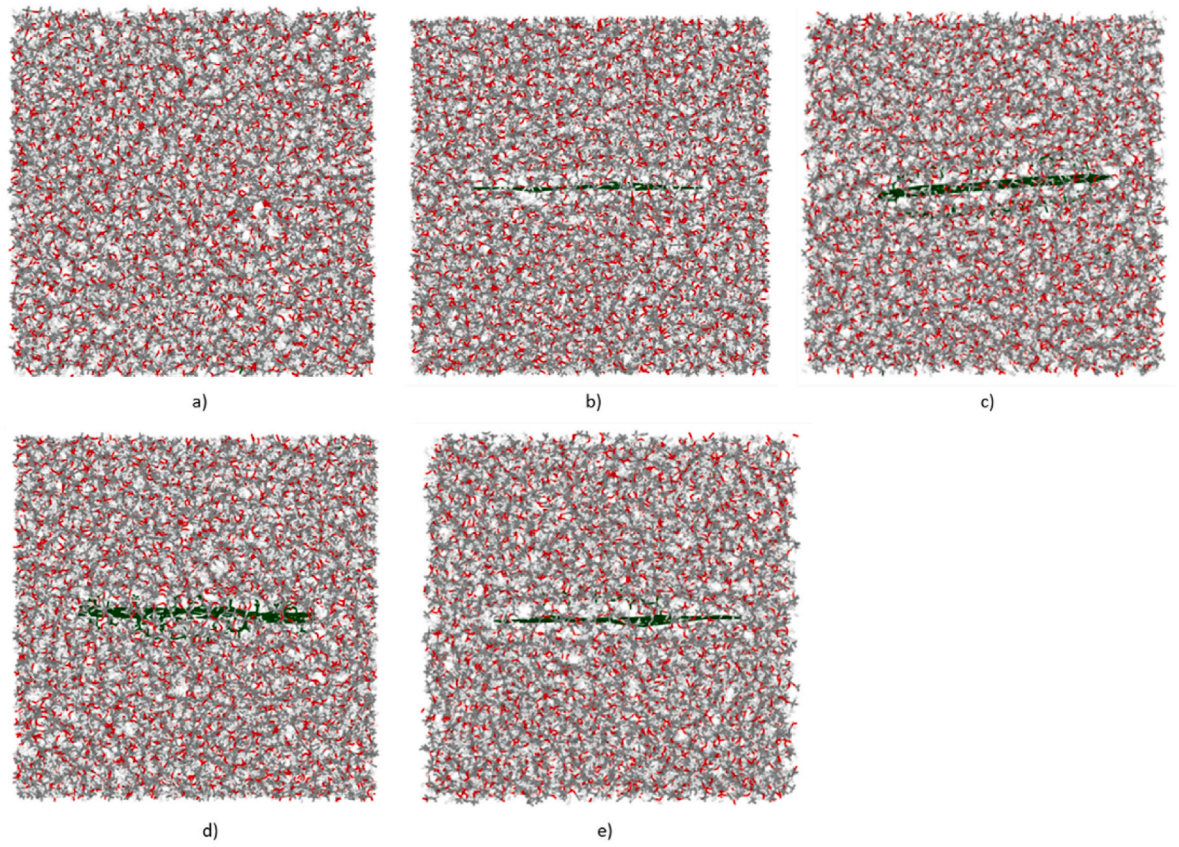

Fig. E1. Representation of the PEG nanocomposites (a) puro PEG, (b) PEG/G, (c) PEG/GNH-1PEG-S, (d) PEG/GNH-1PEG-S-NH_2, (e) PEG/GO-1PEG-S) after equilibration along longitudinal direction. The grey, red, and white colours represent the carbon, oxygen, and hydrogen atoms, respectively. The green colours represent the nanofiller.

References

[1] D. Zhao, et al., Construction of a different polymer chain structure to study π-π interaction between polymer and reduced graphene oxide, Polymers 10 (7) (2018) 716.

[2] A. Díez-Pascual, et al., Recent developments in graphene/polymer nanocomposites for application in polymer solar cells, Polymers 10 (2018) 217.

[3] N. Yousefi, et al., Highly aligned graphene/polymer nanocomposites with excellent dielectric properties for high-performance electromagnetic interference shielding, Adv. Mater. (Weinheim, Ger.) 26 (2014) 5480–5487.

[4] A.C. Balaz, T. Emrick, T.P. Russell, Nanoparticle polymer composites: where two small worlds meet, Science 314 (5802) (2006) 1107–1110.

[5] W. Zheng, B. Shen, W. Zhai, Surface functionalization of graphene with polymers for enhanced properties, in: New Progress on Graphene Research, IntechOpen, London, 2013.

[6] X. Zhang, et al., Facile preparation route for graphene oxide reinforced polyamide 6 composites via in situ anionic ring-opening polymerization, J. Mater. Chem. 22 (2012) 24081–24091.

[7] R.K. Layek, A.K. Nandi, A review on synthesis and properties of polymer functionalized graphene, Polymer 54 (19) (2013) 5087–5103.

[8] F. Banhart, et al., Structural defects in graphene, ACS Nano 5 (1) (2011) 26–41.

[9] D. Cai, M. Song, " Recent advance in functionalized graphene/polymer nanocomposites,", J. Mater. Chem. A 20 (37) (2010) 7906–7915.

[10] J. Cui, et al., A comparative study on enhancement of mechanical and tribological properties of nitrile rubber composites reinforced by different functionalized graphene sheets: molecular dynamics simulations, Polym. Compos. (2020) 1–15.

[11] A. Yadav, A. Kumar, K. Sharma, Determination of elastic constants of functionalizedgraphene-based epoxy nanocomposites: a molecular modeling and MD simulation study, J. Mol. Model. vol 28 (2022) 143.

[12] B. Hu, K. Bi, Interfacial adhesion behavior between conductive polymers and functionalized graphene via molecular dynamic simulation, in: 2020 IEEE 15th International Conference on Nano/Micro Engineered and Molecular System (NEMS), 2020.

[13] Y. Lin, J. Jin, M. Song, Preparation and characterisation of covalent polymer functionalized graphene oxide, J. Mater. Chem. 21 (2011) 3455–3461.

[14] H.J. Salavagione, M.A. Gómez, G. Martínez, Polymeric modification of graphene through esterification of graphite oxide and poly(vinyl alcohol), Macromolecules 42 (17) (2009) 6331–6334.

[15] Z. Xu, C. Gao, In situ polymerization approach to graphene-reinforced nylon-6 composites, Macromolecules 43 (16) (2010) 6716–6723.

[16] S. Güryel, et al., Molecular dynamics simulations of the structure and the morphology of graphene/polymer nanocomposites, Phys. Chem. Chem. Phys. 19 (2017) 12959–12969.

[17] C. Vallés, et al., PMMA-grafted graphene nanoplatelets to reinforce the mechanical and thermal properties of PMMA composites, Carbon 157 (2020) 750–760.

[18] L. Wang, P. Wang, J. Wei, Graphene oxide-graft-poly(l-lactide)/poly(l-lactide) nanocomposites: mechanical and thermal properties, Polymers 9 (2017) 429.

[19] L. Yang, W. Zhen, Synthesis of graphene oxide-polystyrene graft polymer based on reversible addition fragmentation chain transfer and its effect on properties, crystallization, and rheological behavior of poly (lactic acid), Adv. Polym. Technol. 2020 (2020) 16.

[20] L. Chen, et al., Effect of the molecular chains grafted on graphene nanosheets on the properties of poly(l-lactic acid) nanocomposites, Polym. Compos. 38 (1) (2015) 5–12.

[21] Z.S. Pour, M. Ghaemy, Polymer grafted graphene oxide: for improved dispersion in epoxy resin and enhancement of mechanical properties of nanocomposite, Compos. Sci. Technol. 136 (2016) 145–157.

[22] L. Wang, et al., Mechanical and fracture properties of hyperbranched polymer covalent functionalized multiwalled carbon nanotube-reinforced epoxy composites, Chem. Phys. Lett. 706 (2018) 31–39.

[23] F. Liu, et al., The interfacial mechanical properties of functionalized graphene–polymer nanocomposites, RSC Adv. 6 (2016) 66658.

[24] J.R. Gotebiowski, et al., Atomistic QM/MM simulations of the strength of covalent interfaces in carbon nanotube–polymer composites, Phys. Chem. Chem. Phys. 22 (2020) 12007.

[25] Q. Pei, Y. Zhang, V.B. Shenoy, Mechanical properties of methyl functionalizedgraphene: a molecular dynamics study, Nanotechnology 21 (2010) 115709.

[26] Y. Huang, J. Wu, K.C. Hwang, Thickness of graphene and single-wall carbon nanotubes, Phys. Rev. B 74 (2006) 245413.

[27] A. Vashisth, et al., Accelerated ReaxFF simulations for describing the reactive cross-linking of polymers, The Journal of Physical Chemisty A 122 (32) (2018) 6633–6642.

[28] B.D. Jensen, K.E. Wise, G.M. Odegard, The effect of time step, thermostat, and strain rate on ReaxFF simulations of mechanical failure in diamond, graphene, and carbon nanotube, J. Comput. Chem. 36 (21) (2015) 1587–1596.

[29] S. Plimpton, Fast parallel algorithms for short-range molecular dynamics, J. Comput. Phys. 117 (1995) 1–19.
[30] D.H. Tsai, The virial theorem and stress calculation in molecular dynamics, J. Chem. Phys. 10 (3) (1979) 1375–1382.
[31] J.F. Lutsko, Stress and elastic constants in anisotropic solids: molecular dynamics techniques, J. Appl. Phys. 64 (3) (1988) 1152–1154.
[32] J. Cormier, J.M. Rickman, T.J. Delph, Stress calculation in atomistic simulations of perfect and imperfect solids, J. Appl. Phys. 89 (1) (2000) 99–104.
[33] R. Clausius, XVI. On a mechanical theorem applicable to heat, London, Edinburgh Dublin Phil. Mag. J. Sci. 40 (265) (1870) 122–127.
[34] M. Zhou, A new look at the atomic level virial stress: on continuum-molecular system equivalence, Proc. Roy. Soc. Lond.: Math. Phys. Eng. Sci. 459 (2037) (2023) 2347–2392.
[35] A.K. Subramaniyan, C.T. Sun, Continuum interpretation of virial stress in molecular simulations, Int. J. Solid Struct. 45 (14) (2008) 4340–4346.
[36] J.A. Zimmerman, et al., Calculation of stress in atomistic simulation, Model. Simulat. Mater. Sci. Eng. 12 (4) (2004) S319.
[37] Y. Li, et al., Mechanical properties of hydrogen functionalized graphene allotropes, Comput. Mater. Sci. 83 (2014) 212–216.
[38] G. Kacar, Characterizing the structure and properties of dry and wet polyethylene glycol using multi-scale simulations, Phys. Chem. Chem. Phys. 20 (2018) 12303.
[39] Y. Xiang, et al., Molecular dynamics simulations of a poly(ethylene glycol)-Grafted Polyamide membrane and its interaction with a calcium alginate gel, Langmuir 32 (2016) 4424–4433.
[40] G. Kacar, Characterizing the structure and properties of dry and wet polyethylene glycol using multi-scale simulations, Phys. Chem. Chem. Phys. 20 (2018) 12303.
[41] S.J. Stuart, A.B. Tutein, J.A. Harrison, A reactive potential for hydrocarbons with intermolecular interactions, J. Chem. Phys. 112 (14) (2000) 6472–6486.
[42] W.L. Jorgensen, D.S. Maxwell, J. Tirado-Rives, Development and testing of the OPLS all-atom force fieldon conformational energetics and properties of organic liquids, J. Am. Chem. Soc. 118 (1996) 11225–11236.
[43] Z.E. Hughes, et al., Simulation of water transport through functionalized single-walled carbon nanotubes (SWCNTs), J. Phys. Chem. 47 (24943–24953) (2012) 116.
[44] S. Dasetty, J.K. Barrowns, S. Sarupria, Adsorption of amino acids on graphene: assessment of current force fields, in: ChemRxiv, Cambridge Open Engage, Cambridge, 2019, pp. S1–S14.
[45] D. Boda, D. Henderson, The effects of deviations from Lorentz–Berthelot rules on the properties of a simple mixture, Mol. Phys.: An International Journal at the Interface Between Chemistry and Physics 106 (2008) 2367–2370.
[46] A. Kutana, K.P. Giapis, Transient deformation regime in bending of single-walled carbon nanotubes, Phys. Rev. Lett. 97 (2006) 245501.
[47] D. Hossain, et al., Molecular dynamics simulations of deformation mechanisms of amorphous polyethylene, Polymer 51 (25) (2010) 6071–6083.
[48] S. Melchionna, G. Ciccotti, B.L. Holian, Hoover NPT dynamics for systems varying in shape and size, Mol. Phys. 78 (3) (1993) 533–544.
[49] H.D. Ozeren, et al., Prediction of real tensile properties using extrapolations from atomistic, Polymer 228 (2021) 123919.
[50] A. Kubo, J. Albina, Y. Umeno, Construction of master yield stress curves for polycarbonate: a coarse-, Polymer 177 (2019) 84–90.
[51] Effects of temperature and strain rate on the deformation of amorphous polyethylene: a comparison between molecular dynamics simulations and experimental results, Model. Simulat. Mater. Sci. Eng. 21 (2013) 15.
[52] P. Demianenko, et al., Computing thermomechanical properties of dry homopolymers used as raw material for formulation of biomedical hydrogels, J. Mol. Model. 22 (2016) 159.
[53] S.A. Soule, K.V. Cashman, The mechanical properties of solidified polyethylene glycol 600, an analog for lava crust, J. Volcanol. Geoth. Res. 129 (2004) 139–153.
[54] M.A. Nasassrah, F. Podczeck, J.M. Newton, The effect of an increase in chain length on the mechanical properties of polyethylene glycols, Eur. J. Pharm. Biopharm. 46 (1998) 31–38.
[55] R.K. Layek, et al., Amphiphilic poly(N-vinyl pyrrolidone) grafted graphene by reversible addition and fragmentation polymerization and the reinforcement of poly(vinyl acetate) films, J. Mater. Chem. A 1 (2013) 10863.
[56] N. Maity, A. Mandal, A.K. Nandi, Synergistic interfacial effect of polymer stabilized graphene via non-covalent functionalization in poly(vinylidene fluoride) matrix yielding superior mechanical and electronic properties, Polymer 88 (2016) 79–93.
[57] S. Song, C. Wan, Y. Zhang, Non-covalent functionalization of graphene oxide by pyrene-block copolymers for enhancing physical properties of poly(methyl methacrylate), RSC Adv. 5 (2015) 79947–79955.
[58] G.D. Smith, D. Bedrov, Dispersing nanoparticles in a polymer matrix: are long, dense polymer tethers really necessary? Langmuir 25 (19) (2009) 11239–11243.
[59] M. Zheng, X. Li, L. Guo, Algorithms of GPU-enabled reactive force field (ReaxFF) molecular dynamics, J. Mol. Graph. Model. 41 (2013) 1–11.
[60] A. Vasilev, T. Lorenz, C. Breitkopf, Thermal conductivities of crosslinked polyisoprene and Polybutadiene from molecular dynamics simulations, Polymers 13 (2021) 315.
[61] Y. Zhang, et al., Effects of the dispersion of polymer wrapped two neighbouring single walled carbon nanotubes (SWNTs) on nanoengineering load transfer, Compos. B Eng. 45 (1) (2013) 1714–1721.
[62] H. Matsubara, T. Ohara, Effect of the in-plane aspect ratio of a graphene filler on anisotropic heat conduction in paraffin/graphene composites, Phys. Chem. Chem. Phys. 23 (2021) 12082–12092.
[63] A.R. Alian, M.A.N. Dewapriya, S.A. Meguid, Molecular dynamics study of the reinforcement effect of graphene in multilayered polymer nanocomposites, Mater. Des. 124 (2017) 47–57.
[64] B. Faria, N. Silvestre, J.N.C. Lopes, Strength and fracture of graphyne and graphdiyne nanotubes, Comput. Mater. Sci. 171 (2020) 109233.
[65] R. Paberit, et al., Cycling stability of poly(ethylene glycol) of six molecular weights: influence of thermal conditions for energy applications, ACS Appl. Energy Mater. 3 (11) (2020) 10578–10589.
[66] N. Hempel, et al., The influence of temperature and viscosity of PolyethyleneGlycol on the rate of microwave-induced in Situ Amorphization of celecoxib, Molecules 26 (2021) 110.
[67] Y. Li, S. Wang, Q. Wang, Molecular dynamics simulations of thermal properties of polymer composites enhanced by cross-linked graphene sheets, Acta Mech. Solida Sin. 31 (2018) 673–682.
[68] I. Aliyev, et al., Investigation of graphene/graphene oxide reinforced polyurethane nanocomposite: a molecular dynamics approach, Mater. Today: Proceedings 42 (2021) A27–A35.
[69] D.T. Tam, et al., 10 - high-performance ballistic protection using polymer nanocomposites, in: Advances in Military Textiles and Personal Equipment, Woodhead Publishing Series in Textiles, 2012, pp. 213–237.
[70] X. Zhang, et al., A powder-metallurgy-based strategy toward three-dimensional graphene-like network for reinforcing copper matrix composites, Nat. Commun. 11 (2020) 2775.
[71] K. Chenoweth, A.C.T. van Duin, W.A. Goddard, ReaxFF reactive force field for molecular dynamics simulations of hydrocarbon oxidation, J. Phys. Chem. 112 (5) (2008) 1040–1053.